AD-A104 180 ADVANCED RESEARCH AND APPLICATIONS CORP SUNNYVALE CA F/G 20/12
INVESTIGATION OF IMPURITY REDISTRIBUTION EFFECTS AND SOLUBILITY--ETC(U)
JUN 81 T J MAGEE, C LEUNG, R ORMOND N00014-80-C-0482
UNCLASSIFIED NL

1 OF 2
AD A
104180

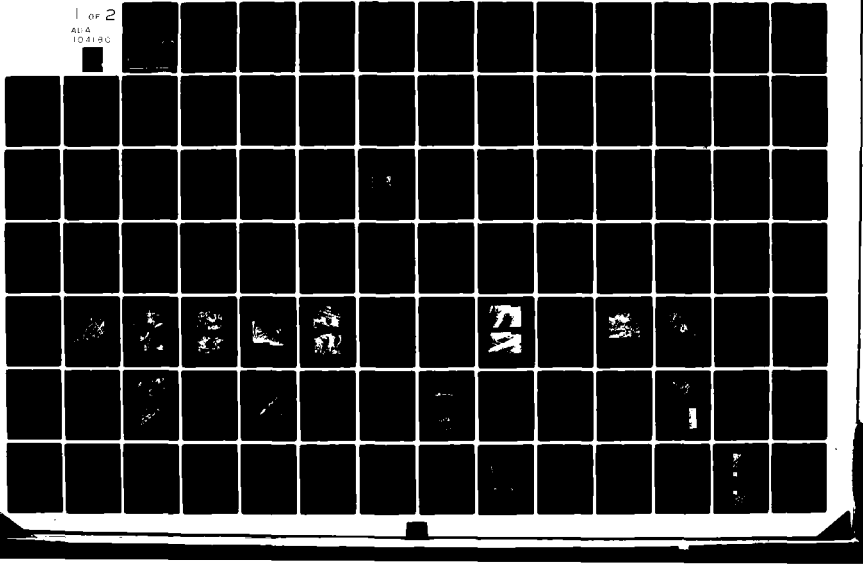

ARACOR

LEVEL II

AN INVESTIGATION OF IMPURITY REDISTRIBUTION EFFECTS AND SOLUBILITY/DIFFUSIVITY OF Cr IN GaAs

INTERIM TECHNICAL REPORT

BY

T. J. MAGEE

PREPARED FOR:

DEFENSE ADVANCED RESEARCH PROJECTS AGENCY
1400 WILSON BOULEVARD
ARLINGTON, VIRGINIA 22209

ATTENTION: MR. S. ROOSILD

MONITORED BY:

OFFICE OF NAVAL RESEARCH
DEPARTMENT OF THE NAVY
800 NORTH QUINCY STREET
ARLINGTON, VIRGINIA 22217

ADVANCED RESEARCH AND APPLICATIONS CORPORATION

UNCLASSIFIED

SECURITY CLASSIFICATION OF THIS PAGE (When Data Entered)

REPORT DOCUMENTATION PAGE

READ INSTRUCTIONS BEFORE COMPLETING FORM

1. REPORT NUMBER	2. GOVT ACCESSION NO.	3. RECIPIENT'S CATALOG NUMBER
	AD-A104	180

4. TITLE (and Subtitle)

INVESTIGATION OF Cr REDISTRIBUTION EFFECTS AND SOLUBILITY/DIFFUSIVITY OF Cr IN GaAs

5. TYPE OF REPORT & PERIOD COVERED

Interim Report, 1 Nov. 1980 to 1 May 1981

6. PERFORMING ORG. REPORT NUMBER

7. AUTHOR(s)

T.J. Magee, C. Leung, R. Ormond, R.A. Armistead
D. Stevenson*, ~~C.A. Evans, Jr., D.S. Day + and~~
M. Omuri+
*Stanford University +Avantek, Inc.

8. CONTRACT OR GRANT NUMBER(s)

N00014-80-C-0482 New

9. PERFORMING ORGANIZATION NAME AND ADDRESS

Advanced Research & Applications Corporation
1223 East Arques Avenue
Sunnyvale, Ca 94086

10. PROGRAM ELEMENT, PROJECT, TASK AREA & WORK UNIT NUMBERS

PE 61101E
Project ~~0D10~~
Task NR 243-031

11. CONTROLLING OFFICE NAME AND ADDRESS

Defense Advanced Research Projects Agency
Materials Sciences Office
1400 Wilson Blvd., Arlington, VA 22209

12. REPORT DATE	13. NO. OF PAGES
June 1, 1981	95

14. MONITORING AGENCY NAME & ADDRESS (if diff. from Controlling Office)

Office of Naval Research
Code 427, M. Yoder
Arlington, VA 22217

15. SECURITY CLASS. (of this report)

Unclassified

15a. DECLASSIFICATION/DOWNGRADING SCHEDULE

16. DISTRIBUTION STATEMENT (of this report)

Approved for public release; distribution unlimited.

17. DISTRIBUTION STATEMENT (of the abstract entered in Block 20, if different from report)

18. SUPPLEMENTARY NOTES

ONR Scientific Officer
Telephone: (202)696-4218

19. KEY WORDS (Continue on reverse side if necessary and identify by block number)

Gallium arsenide	Diffusion	Epitaxial layers
Defect gettering	Impurity effects	Reliability
Impurity gettering	Electrical contacts	
Semiconductors	Annealing	
Field effect transistors	Implantation damage	

20. ABSTRACT (Continue on reverse side if necessary and identify by block number)

Experiments have begun on the investigation of the thermodynamics and phase equilibrium of the Ga-Cr-As system and the solubility and diffusivity of Cr in GaAs under selected conditions of temperature and source composition. Allied experiments on the influence of defects in GaAs have shown the stable front surface of Cr depletion channels can be formed in GaAs for retarding the outdiffusion of Cr. Investigations of the influence of non-stoichiometric regions introduced by implantation (as predicted by the Christel-Gibbons model)

DD FORM 1 JAN 73 1473

EDITION OF 1 NOV 65 IS OBSOLETE

UNCLASSIFIED 393004

SECURITY CLASSIFICATION OF THIS PAGE (When Data Entered)

- on the redistribution of Cr after annealing have shown a definitive correlation between predicted damage zones and experimentally observed gettering regions.

The field-enhanced diffusion of Cr into contact regions of GaAs-FETs under accelerated thermal-bias stress testing has now been shown to be correlated with the degradation of contacts during stress.

Separate experiments of CZ-Si (containing oxygen) have shown that oxygen is extremely mobile in back surface damaged regions and ion implanted junctions of Si wafers. Motion and gettering of ^{16}O into processing regions has been demonstrated at annealing temperatures as low as 350°C.

Evaluations of CdTe, HgCdTe and LPE-HgCdTe/CdTe samples currently used in IR detector fabrication have shown extreme variability in the concentrations of defects, precipitation and propagation of defects into active device regions.

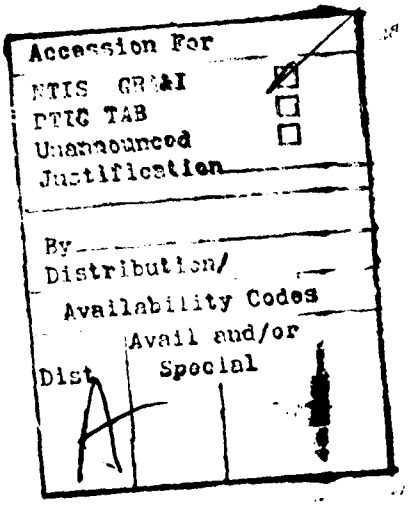

CONTENTS

FIGURES

TABLES

1. INTRODUCTION

1.1 BACKGROUND

Gallium arsenide (GaAs) device fabrication requires semi-insulating substrates. In order to achieve high resistivities in GaAs substrates, the effects of impurities and deep level traps within the material must be compensated. These impurities have been successfully compensated by Cr additions to achieve resistivities $\geq 10^7$ Ω-cm in GaAs. However, recent investigations have shown that the behavior of Cr has not been properly understood and a number of problems occuring during GaAs device fabrication can be attributed, in part, to the anomalous redistribution of Cr both during and subsequent to thermal processing.

In 1978, experiments within the United Kingdom by Tuck et al. using radiotracers showed that Cr diffuses readily in GaAs at temperatures in the range 720°C to 750°C, resulting in outdiffusion from the substrate into epitaxial layers grown on semi-insulating wafers. Their data suggested the diffusion of Cr cannot be explained by a simple substitutional motion and rather, an interstitial mechanism must be employed.

During the same period, independent experiments in the United States by T.J. Magee et al. on optimized back-surface-damaged GaAs samples showed that Cr was mobile at 750°C and could rapidly gettered within damaged regions in the range 650°C to 750°C. Subsequent experiments showed that Cr could also be gettered by damage introduced in the GaAs during implantation of active impurities such as Se or S and that stresses introduced by the encapsulant at the interface would also getter Cr. These results partially explain the often observed existence of "dead" layers in ion-implanted (capped) samples after annealing.

Following these initial experiments, investigations by researchers at Hughes Research Laboratory, Rockwell International and Hewlett Packard have confirmed the redistribution behavior of Cr during thermal processing. However, detailed experiments to investigate the solid solubility of Cr in GaAs, to quantify diffusion constants and to determine the influence of lattice defects on diffusion have not as yet been performed. Equally lacking is information on the influence of other impurities such as C, O, and B (typically included in LEC material). Detailed analyses of the effect of dopants, such as Si, Sn, Se, S, or Te, on Cr diffusion have also not been performed, although preliminary experiments by our group on Sn-doped LPE layers and Si-doped VPE layers showed that the diffusion of Cr within the epitaxial layers is markedly altered.

Of additonal interest is the possible correlation between contact degradation and Cr diffusion during accelerated thermal stress-bias testing of devices. Initial research reported by ARACOR has shown that Cr redistributes and getters into contact regions during the alloying sequence. At that time, it was suggested that Cr redistribution was possibly responsible for long-term contact degradation during accelerated life testing. However, no experiments have been reported on the combined role of electric field and thermal stress on the redistribution of Cr and its effect of contact failure.

The objective of this program is to provide a detailed investigation of the role of defects and impurities in the GaAs lattice, with particular emphasis on the behavior of Chromium. The program includes a study of the thermo-dynamics and phase equilibrium of the Ga-Cr-As system; an investigation of the solubilities of Cr in GaAs under selected

conditions of temperature and source composition; and measurements of the diffusivity if Cr in GaAs, with emphasis on the diffusion of Cr in a concentration gradient. In addition, the role of defects and resolvable complexes will be investigated in relation to Cr-difffusion. The role of defects, bias-voltage (field) and additional dopants will also be investigated to determine the possible relationship between Cr diffusion and electric field in relation to contact degradation.

In this report we will summarize briefly the progress attained during the first 12 months. In addition, we will discuss preliminary data obtained on the quality and microstucture in CdTe and HgCdTe material used in IR detector fabrication. In the sections following, we will also present data obtained on the redistribution of oxygen in Si oxygen in Si, particularly within near surface regions under simulated processing conditions.

1.2 SUMMARY OF RESULTS

During the first six months period of this program, the following results have been obtained:

- o Investigation of front surface Cr depletion channels formed by B implantation into GaAs and subsequent annealing in arsine.
- o Investigation of electrical transport properties within Cr depletion channels in GaAs.
- o Preliminary investigations of the low temperature stress-bias degradation of ohmic contacts on GaAs FET devices.

- o Identification of field enhanced diffusion of Cr in GaAs.

- o Investigation of the Cr-Ga, As-Cr systems, DTA measurements and surface degradation studies in Cr-doped GaAs.

- o Initial evaluation of CdTe and HgCdTe substrates used in IR detector fabrication.

- o Initial experiments on the enhanced diffusion of oxygen in Si in the presence of microstructural damage.

- o Improved techniques for stabilizing back surface gettering in Si

- o Redistribution of oxygen in Si during solid phase regrowth of As-implanted, amorphized Si

- o Low temperature redistribution of oxygen into ion implanted regions

- o Role stabilized back surface damage in controlling internal SiOx precipitation in Si

1.3 PUBLICATIONS

The following publications were drawn in part or in total from this program of research:

a) "Incorporation of Boron During the Growth of GaAs Single Crystals," Applied Physics Letters 36, June 15, 1980 (pp.989-990).

b) "Low Temperature Gettering of Cr in GaAs," Applied Physics Letters 37, July 1, 1980 (pp.53-55).

c) "Annealing of Damage and Redistribution of Cr in Boron-Implanted, Si_3N_4 Capped GaAs," Applied Physics Letters 37, Sept. 1, 1980 (pp. 447-449).

d) "Low Temperature Redistribution of Cr in Boron-Implanted GaAs in the Absence of Encapsulant Stress," Applied Physics Letters 37, Oct. 1, 1980 (pp. 635-637).

e) "Front Surface Control of Cr Redistribution and Formation of Stable Cr Depletion Channels in GaAs," Applied Physics Letters 38,April,1981 (pp.559-561).

f) "Gettering of Mobile Oxygen and Defect Stability Within Back-Surface Damage Regions in Si", Applied Physics Letters (June 1,1981).

g) "Low Temperature Redistribution and Gettering of Oxygen In Silicon", (submitted - Journal of Applied Physics, 1981).

h) "Thermal Redistribution of Oxygen During Solid Phase Regrowth of As-Implanted, Amorphized Si," (submitted - Applied Physics Letters, 1981).

i) "Redistribution of Oxygen Within Damage Regions of Boron Implanted Silicon", (submitted - Applied Physics Letters, 1981).

1.4 TECHNICAL PRESENTATIONS

a) Process Technology for Direct Ion Implantation in Semi-Insulating III-V Materials-Workshop, University of California, Santa Cruz, August 12-13, 1980.

1) "Gettering of GaAs Wafers for Impurity and Defect Control"
2) "Front Surface Control of Cr Redistribution and Formation of Stable Cr Depletion Channels in GaAs"

b) DARPA-HgCdTe Materials Processing Research Program Review, Dec. 17-18, 1980, Washington, D.C. - "Defects in HgCdTe and CdTe as observed by Transmission Electron Microscopy".

c) Workshop on Compound Semiconductor Materials and Microwave Devices, February, 1980, New Orleans, La. - "Field Enhanced Diffusion of Cr and Contact Degradation".

d) Ad-Hoc Electronics Committee, DoD/DARPA, May, 1981, Washington, D.C.,"Physical Characterization of Si Wafers".

2. FRONT SURFACE CONTROL OF Cr REDISTRIBUTION AND FORMATION OF STABLE Cr DEPLETION CHANNELS IN GaAs.

Over the past two years it has been demonstrated that Cr is rapidly redistributed in GaAs at temperatures in the range 300° to 1000°C, using established encapsulation procedures and capless techniques during annealing[1-8]. However, there have been no reported investigations on methods for controlling Cr redistribution at the surface or within ion implanted regions of GaAs.

In recent papers,[9,10] we discussed the development of Cr-depletion regions in B-implanted GaAs annealed in flowing H_2 both in the presence of an Si_3N_4 encapsulatant and in the absence of an encapsulating layer. This section presents correlated data from secondary ion mass spectrometry (SIMS), capacitance-voltage (C-V) and Hall effect measurements showing the formation, control and stability of Cr-depletion zones created in B-implanted GaAs after annealing in arsine and the development of stable n-type conduction across the depletion channel.

Gallium arsenide wafers used in this study were of (100) orientation and grown by the Bridgman technique. Background Cr-doping levels were in the range, 4×10^{16} to 2×10^{17} atoms-cm^{-3}. After cleaning, the GaAs wafers were implanted with 100 keV B-ions to a dose of 5×10^{14} ions cm^{-2}. Annealing was done in a horizontal quartz reactor tube with a quartz wafer holder. A flowing gas mixture of Pd-diffused H_2 (400 cc/min.) and 5% AsH_3 in H_2 (20 cc/min.) was used for the required annealing temperatures ($T_A \leq 850°C$). For T_A = 900°C, the AsH_3/H_2 flow rate was increased to 30 cc/min. Under these conditions, a partial pressure of arsenic was produced in excess of the equilibrium partial pressure of arsenic at the GaAs surface[11] and was shown to be adequate for the range of annealing temperatures used in this study.

Carrier concentration profiles were obtained from differential capacitance-voltage (C-V) measurements using a Shandon Southern Impurity Profile Plotter and Hg probes for making contacts to the wafer. Hall effect/sheet resistivity measurements were made using the standard van der Pauw technique[12]. Carrier concentration depth profiles were obtained using acid layer removal and Hall effect measurements. Incremental layers were removed by immersing samples in an NH_4OH: H_2O_2: H_2O (2:1:100) solution, producing an etching rate of 30A/sec.

Samples for SIMS profiling analyses were prepared in the form of 5 mm squares. Both control (no implantation) and implanted samples subjected to similar annealing schedules were investigated to provide comparative information on Cr-redistribution. A Cameca IMS-3f ion microanalyzer with O_2 primary ion bombardment and positive secondary ion spectroscopy was used for impurity profiling. Atomic concentrations of Si, Cr, B and other impurities were calibrated using standards prepared by ion implantation into GaAs substrates.

Secondary ion mass spectrometry profiles of the Cr-impurity distribution within control (not implanted) wafers used in these experiments showed no significant surface redistribution of Cr after annealing in arsine at temperatures $\leq$850°C. In Fig. 1 we show representative SIMS profiles obtained from separate samples of the B and Cr concentrations after B implantation and subsequent annealing in arsine for 1 hour at temperatures of 650°C, 750°C and 800°C. Also shown for reference are SIMS profiles of the Cr distributions in implanted (unannealed) and control (annealed, not implanted) samples. At temperatures <850°C, we observe no detectable diffusion of the implanted B, in agreement with earlier results.[9,10,13] In Figure 1a), after annealing at 650°C

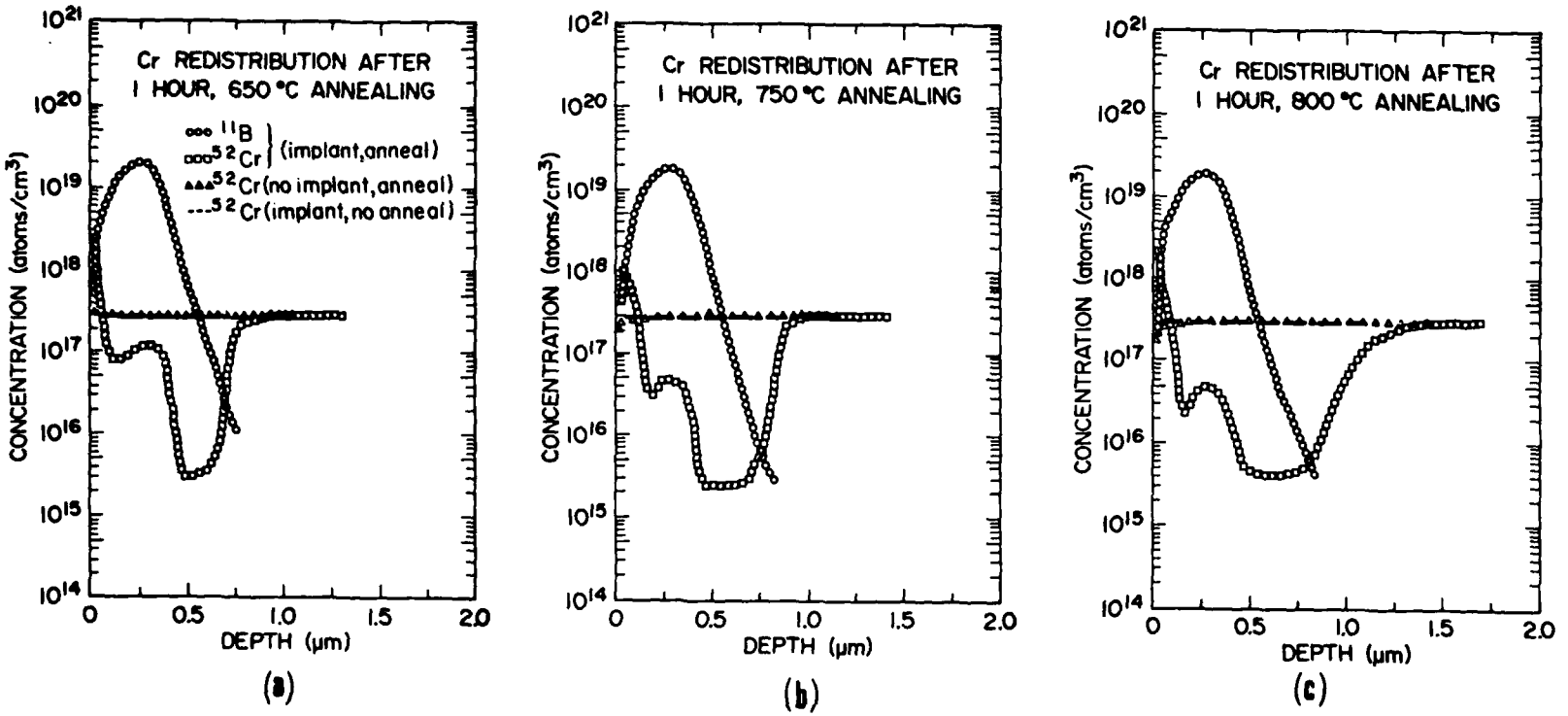

FIG. 1. SIMS PROFILES OF B AND Cr CONCENTRATIONS AFTER IMPLANTATION OF B AND SUBSEQUENT ANNEALING IN ARSINE AT VARIABLE TEMPERATURES FOR L HR: (a) 650°C; (b) 750°C; (c) 800°C. CHROMIUM CONCENTRATION PROFILES ARE ALSO SHOWN FOR REFERENCE IN IMPLANTED (UNANNEALED) AND ANNEALED (UNIMPLANTED) CONTROL SAMPLES.

we observe a rapid depletion and subsequent motion of Cr toward the surface, creating a zone of Cr depletion and a relatively sharp shoulder at $\simeq$ 0.75 μm. As the temperature is increased to 750°C (Figure 1b) the Cr depletion zone expands inwards forming a buried channel zone $\simeq$ 0.5 μm in width. At the outer edge of the channel, gettered Cr is present within damage regions at R_p, the projected range. At 800°C, the amount of Cr gettered within damage at R_p is further decreased, accompanied by additonal motion of Cr toward the surface and an increase in the effective width of the depletion channel (Fig.1c).

The Cr redistribution shown in Figure 1 is in sharp contrast to the results observed with implants of heavier ions in GaAs after annealing at temperatures $\leq$850°C.[2,7,14] For temperatures > 850°C, we detected a breakdown of the channel region and an annihilation of effective pinning of Cr at the edge of the implanted B-distribution. The resulting Cr distribution (T_A >850°C) is then similar to profiles observed in previous experiments[9,13] and is characterized by the presence of a long depletion tail extending to a depth of 2 μm. From these results we can conclude that the thermal stability limit for channel definiton and Cr control is reached at anneal temperatures of <850°C.

To further extend these results, we performed a similar set of experiments using samples containing a Cr background concentration of 4×10^{16} atoms cm^{-3}. In Fig. 2, we show the Cr redistribution profile obtained after implantation and annealing at 750°C. Of particular interest is the formation of a well-defined "square well" Cr depletion channel extending to a depth $\simeq$ 1 μm from the surface. These experiments were repeated on a number of samples and essentially identical Cr redistribution profiles obtained. In agreement with the previous data, we observed a (channel) thermal stability limit at 850°C.

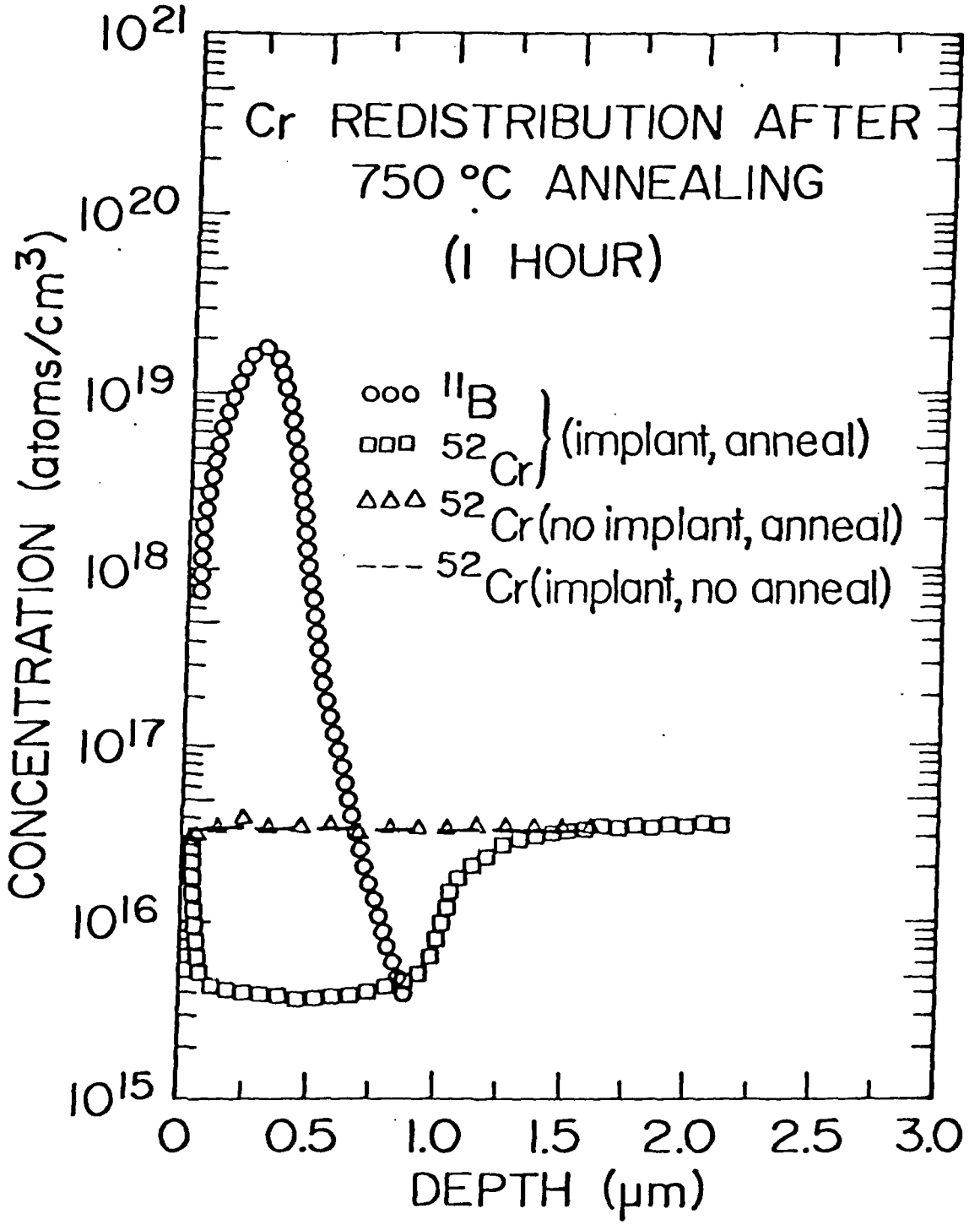

FIG. 2. SIMS PROFILES OF B AND Cr CONCENTRATIONS IN LOW (4×10^{16} ATOMS CM^{-3})-Cr-CONTENT GaAs WAFER AFTER B IMPLANTATION AND SUBSEQUENT ANNEALING IN ARSINE AT 750°C FOR 1 HR. ALSO SHOWN FOR REFERENCE ARE THE Cr CONCENTRATION PROFILES OBTAINED FROM IMPLANTED (UNANNEALED) AND ANNEALED (UNIMPLANTED) CONTROL SAMPLES.

To obtain information on possible conduction across the depletion channel in the presence of the implanted B distibution, we obtained C-V and Hall effect/stripping measurements on the implanted, annealed samples. In Fig.3, we show the electron concentrations and mobilities obtained at substrate temperatures of 77°K and 300°K for Hall effect measurements and 300°K for C-V measurements. Comparing the data of Figures 2 and 3, we observe that the maximum carrier concentration ($\simeq 10^{16}$ cm^{-3}) extends to a depth of $\simeq$ 0.8 μm and is reduced rapidly at the edge of the Cr depletion channels. Since the background Si concentration determined from SIMS analyses was $\simeq$ 1.6 x 10^{16} atoms cm^{-3} and the net donor (N_D-N_A) atom concentration was $\simeq 10^{16}$ atoms cm^{-3}, we can conclude that Si impurities in the GaAs are primarily responsible for conduction across the Cr-depletion zone.

Of interest is the fact that Hall mobilities were 5200 and 11600 cm^2/V-sec across the depletion channel at 300° and 77°K, respectively, in the presence of residual damage retained within the B-implantation region after annealing[9,10]. Since the peak B concentration was $\simeq 10^{19} cm^{-3}$, and $\simeq 10^{16}$ carriers/cm^3 (background impurities) were detected across the B-implanted, Cr-depleted channel, it is apparent that boron does <u>not</u> significantly contribute to compensation in the GaAs lattice under the experimental conditions employed.

From the data obtained we can conclude that Cr-depleted channels can be created in GaAs using B-implantation and subsequent annealing in <u>arsine</u>. Pinning of Cr at the edge of the implanted B distribution occurs reproducibly and appears to be stable for anneal temperatures <850°C. Although the present experimental data do not permit an exact description of the depletion and pinning mechanisms, we can speculate that the diffusion of Cr within the implanted region is

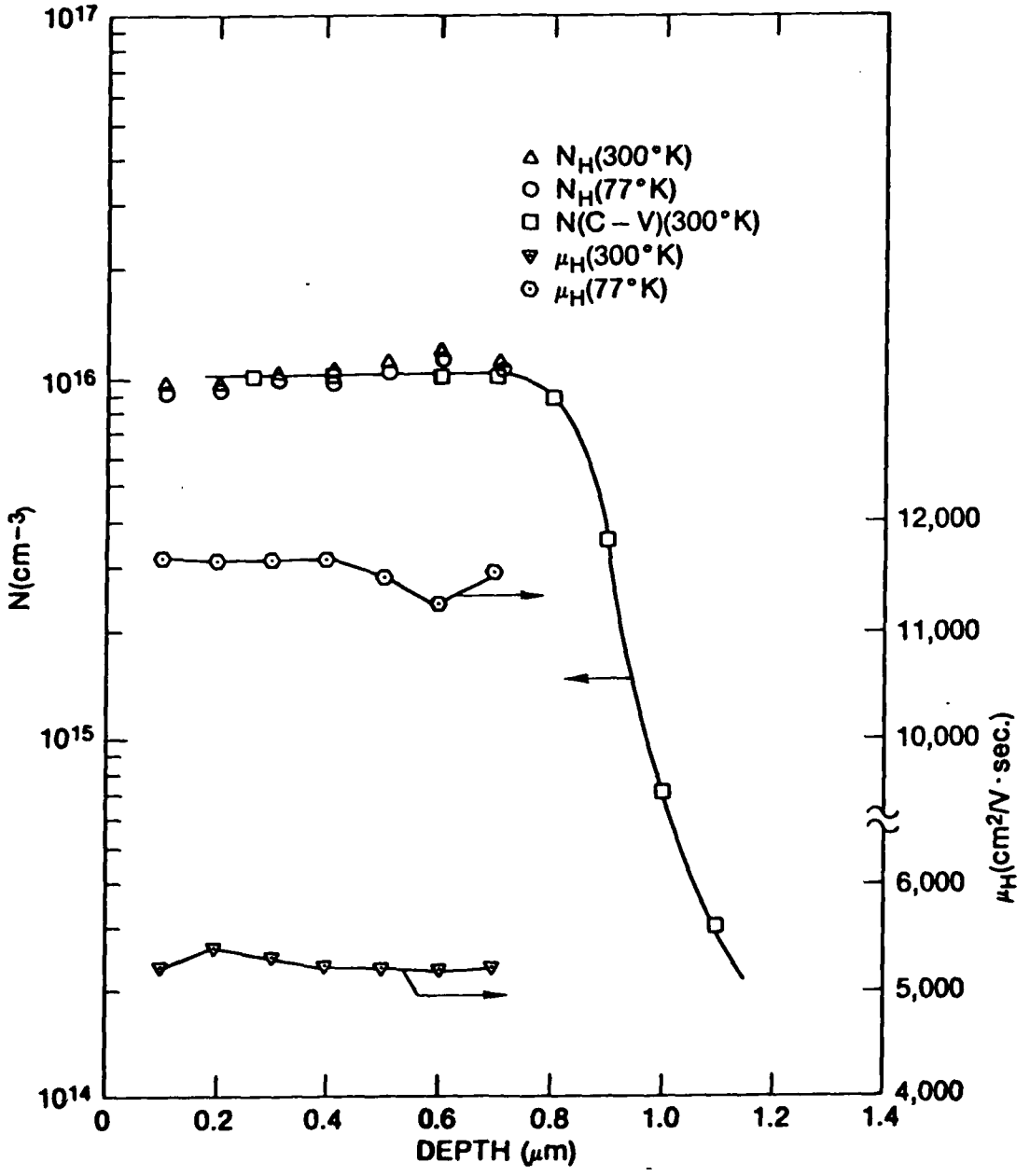

FIG. 3. ELECTRICAL PROFILES OBTAINED FROM C-V AND HALL-EFFECT/STRIPPING MEASUREMENTS AT SUBSTRATE TEMPERATURES OF 77 AND 300K. ELECTRON CONCENTRATIONS AND HALL MOBILITIES ARE PLOTTED AS A FUNCTION OF DEPTH FROM THE SURFACE OF THE GaAs.

enhanced in the presence of implant damage and the redistribution of Cr correlated with the annealing of microstructural defects[9]. As the anneal temperature is increased above 500°C, Cr outdiffuses readily to the surface, creating a well defined channel and abrupt shoulder at the two edges of the boron distribution. In the presence of an implanted B impurity gradient, diffusion within the depletion channel is possibly retarded at these temperatures because of changes in the Cr diffusion coefficient. If indeed valid, this would explain the creation of the sharply defined shoulder in the Cr-distribution profile, but additional experiments are needed to provide definitive information.

It is conceivable that the observed phenomena may be useful for device applications, particularly for charged coupled devices, where a sharp depletion shoulder on the Cr distribution would be desirable.[15] Activation of secondary ion implanted impurities within the depletion channel should also be possible; however, it is felt that the boron dose level must be reduced to permit activation of ion implants ($\approx 10^{17} cm^{-3}$) used in device fabrication. Experiments are continuing and the results will be reported at a later date.

3. CONTROL OF Cr OUTDIFFUSION INTO VPE LAYERS ON GaAs

In the previous chapter we discussed the use of B-implantation to create stable Cr depletion channels in GaAs and showed that the creation of such channels might be useful for fabrication of devices using the sharply defined channel region for a conduction channel.

Since the Cr is effectively pinned by the implanted B distribution and the effect appears thermally stable to temperatures <850°C, we decided to investigate this technique to determine if the amount of Cr outdiffusion could be reduced during VPE growth of layers on semi-insulating wafers.

Semi-insulating GaAs wafers were implanted with 300keV B^{+} ions to a dose of $5x10^{14}/cm^{2}$ and subsequently annealed in arsine, wafers were loaded into a VPE reactor and heated to the deposition temperature of 720°C. Following a brief vapor etch, undoped 2 m thick GaAs layers were grown, using a standard hydride (AsH_3 + HCl + Ga) reactor typically used for production of GaAs layers for MESFET requirements.

It was found initially athat control of the "etch-back" step prior to growth of the VPE layers was a critical factor. If the etch-back depth was close to the shoulder of the Cr distribution (Fig. 2) normal Cr outdiffusion would occur. After a series of experiments we were able to adequately control the etch back depth and produce suitable layers on GaAs.

Figure 4, shows SIMS profiles of the B and Cr distributions obtained after epitaxial growth on the GaAs substrate containing a Cr depletion channel. It can be observed that

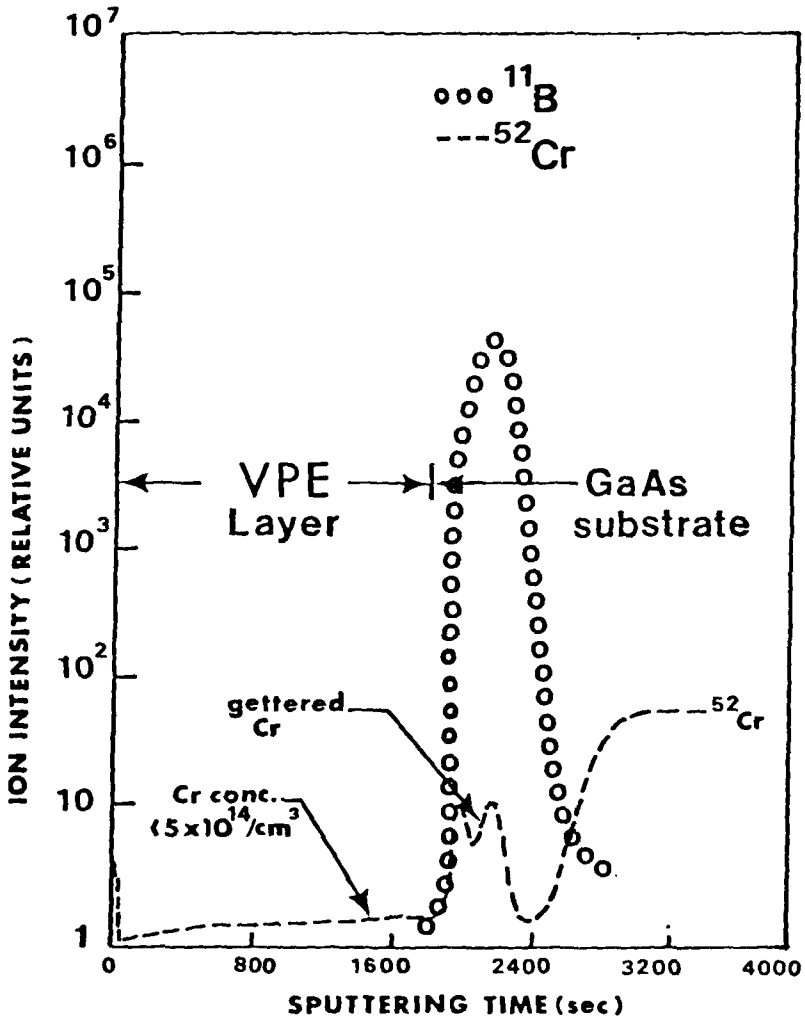

FIG. 4. SIMS PROFILES OF B AND Cr CONCENTRATIONS IN VPE LAYER GROWN ON B-IMPLANTED, ANNEALED GaAs SUBSTRATE.

the Cr depletion channel is essentially retained during VPE layer growth at 720°C. Small amounts of diffusing Cr are gettered within damage zones of the implanted region and forward diffusion of Cr across the interface is retarded. The asymmetry of the implanted B-distribution observed is caused by the etch-back step, prior to VPE growth, thereby removing a portion of the surface layer. Chromium levels in the VPE layer are dramatically reduced, resulting in measured concentrations $<5\times10^{14}/cm^3$. Subsequent measurements in the fast-profiling mode have established the Cr concentration at $3\times10^{14}/cm^3$ within the epilayer. This concentration level is currently equal to or lower than that reported for some of the better LEC crystals grown. In addition, this is the lowest Cr concentration ever obtained within epitaxial layers on Cr-doped S.I. substrates, including results obtained using LPE, VPE, MBE and MOCVD growth techniques.

Since the crystalline perfection of the epitaxial layers (active region) is generally better than bulk wafers grown by the LEC technique, it would now be interesting to determine if FET device performance can be improved in the presence of low Cr levels and reduced defect densities. In ealier studies conducted by NRL it has been suggested that transient radiation susceptibility is related to Cr doping level. Furthermore, in the sections to follow, we will discuss the problem of field enhanced diffusion of Cr in GaAs and the correlation with contact degradation. If the Cr level can be reduced, as shown in the current experiments, it is feasible to assume that contact reliability and radiation hardness can be improved. Experiments in these areas are continuing and the results will be reported at a later date.

4. CHROMIUM REDISTRIBUTION AND STOICHIOMETRY DISTURBANCES IN ION IMPLANTED GaAs

In earlier papers we have shown that Cr is redistributed rapidly at temperatures of 400° to 500° in B-implanted GaAs in the absence of an encapsulating layer. Of particular interest in these studies is the fact that initial Cr depletion and gettering does not occur at depths equal to the projected range, Rp, where the maximum concentration of implant damage would be expected, but at depths exceeding Rp.

In recent studies, Christel and Gibbons have shown that ion implantation into compound semiconductors produces not only a characteristic damage region, but a non-stoichiometric distribution of the host atoms. Because of the differing masses of the Ga and As, the collision cross section, maximum energy transfer and recoil range distribution for each of the elements will be different, producing a varying Ga/As ratio as a function of depth into the sample, suggesting the possibility of interstitial concentrations at depths exceeding Rp.

In Fig. 5, we show the calculated profiles (after Christel and Gibbons) for an implanted B-distribution (50keV, $10^{15}/cm^2$) with the Ga-As vacancy concentration profiles and net Ga-As displacement plotted as a function of depth. It is of interest to note that the interstitial concentration profiles (net Ga-As displacements) occur at depths exceeding R_p and stoichiometric imbalance is produced at varying depths from the surface.

To further investigate the possible correlation between these predicted stoichiometric disturbances and Cr redistribution, we implanted B at energies of 50, 100 and 300 keV into Bridgman grown GaAs samples (in separate experiments)

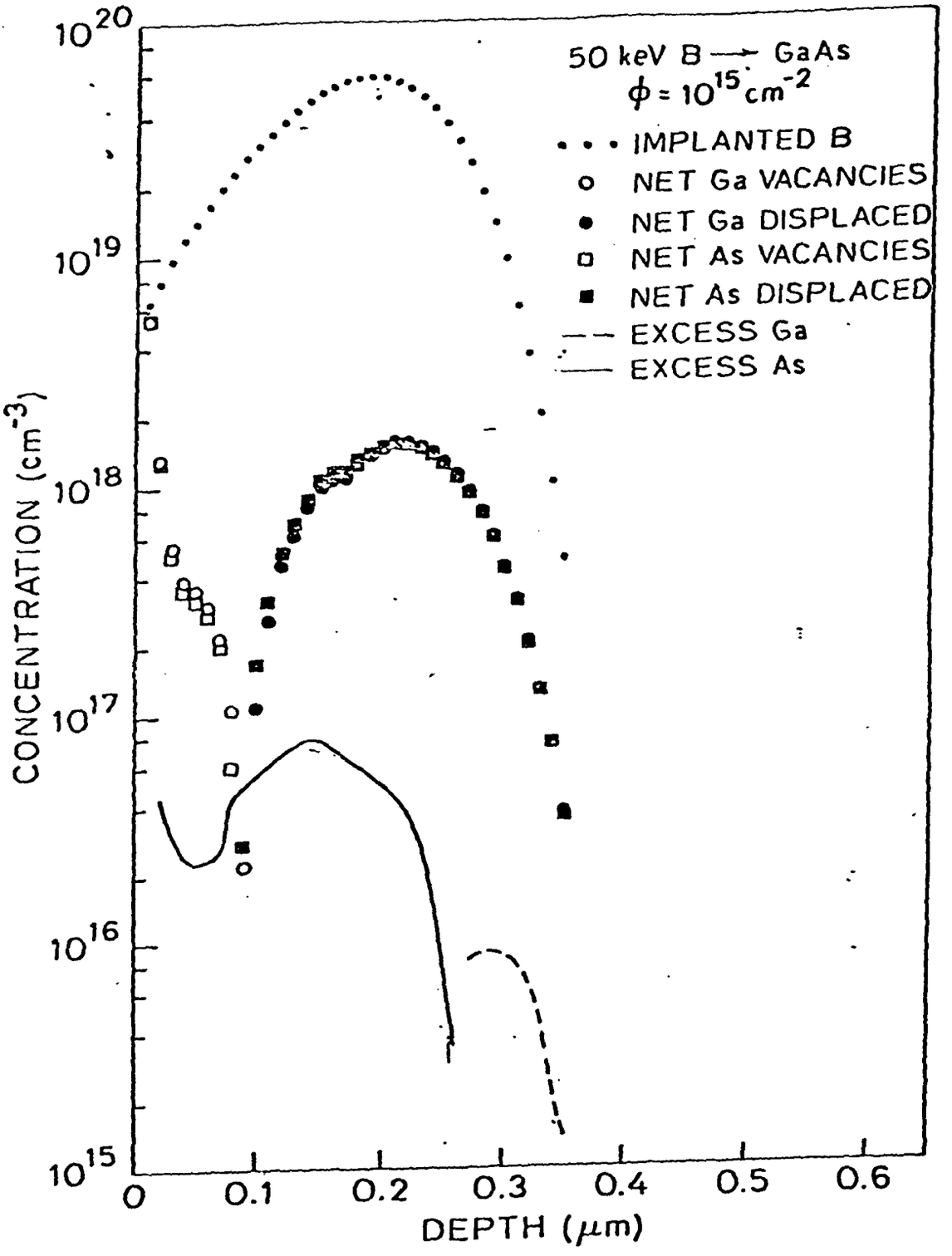

FIG. 5. NET Ga/As VACANCIES AND NET Ga/As DISPLACED FOR 50KeV B-IMPLANT INTO GaAs

to total doses of 10^{15}ions/cm^2. In Fig. 6 we show the Cr redistribution profiles obtained on 50 keV B-implanted (10^{15}/cm^2) GaAs samples subsequent to annealing (capless) in flowing H_2 at 500°C for 1 hr. Also shown for reference are the Christel-Gibbons calculated Ga-As vacancy and interstitial profiles after implantation. It can be observed that initial depletion and gettering of Cr occurs approximately at the edge and peak of the calculated interstitial profile, respectively. Under these annealing conditions and in the absence of an encapsulating layer, near-surface redistribution of Cr is essentially absent, as indicated in the figure.

Correlated TEM data obtained on the implanted annealed samples show a distribution of dislocation loops within the peak region of the predicted interstitial concentration and into the damage region at Rp. From this data, we can conclude that the interstitials produced during implantation are clustered (after annealing) in the form of observable dislocation loops. Gettering of Cr occurs within this zone in the presence of the interstitial clusters. Interaction and pinning of Cr at the edge of dislocation loops has been discussed in a number of earlier papers, although such discussions have been limited to the gettering of Cr by residual structure within damage zones at Rp.

To extend these results, we also performed a series of tests on samples implanted at 100 and 300 keV to similar dose levels and annealed under the same conditions. Preliminary data show that a similar pattern of Cr distribution and gettering is observed, with interstitial loop concentrations present at depths > Rp.

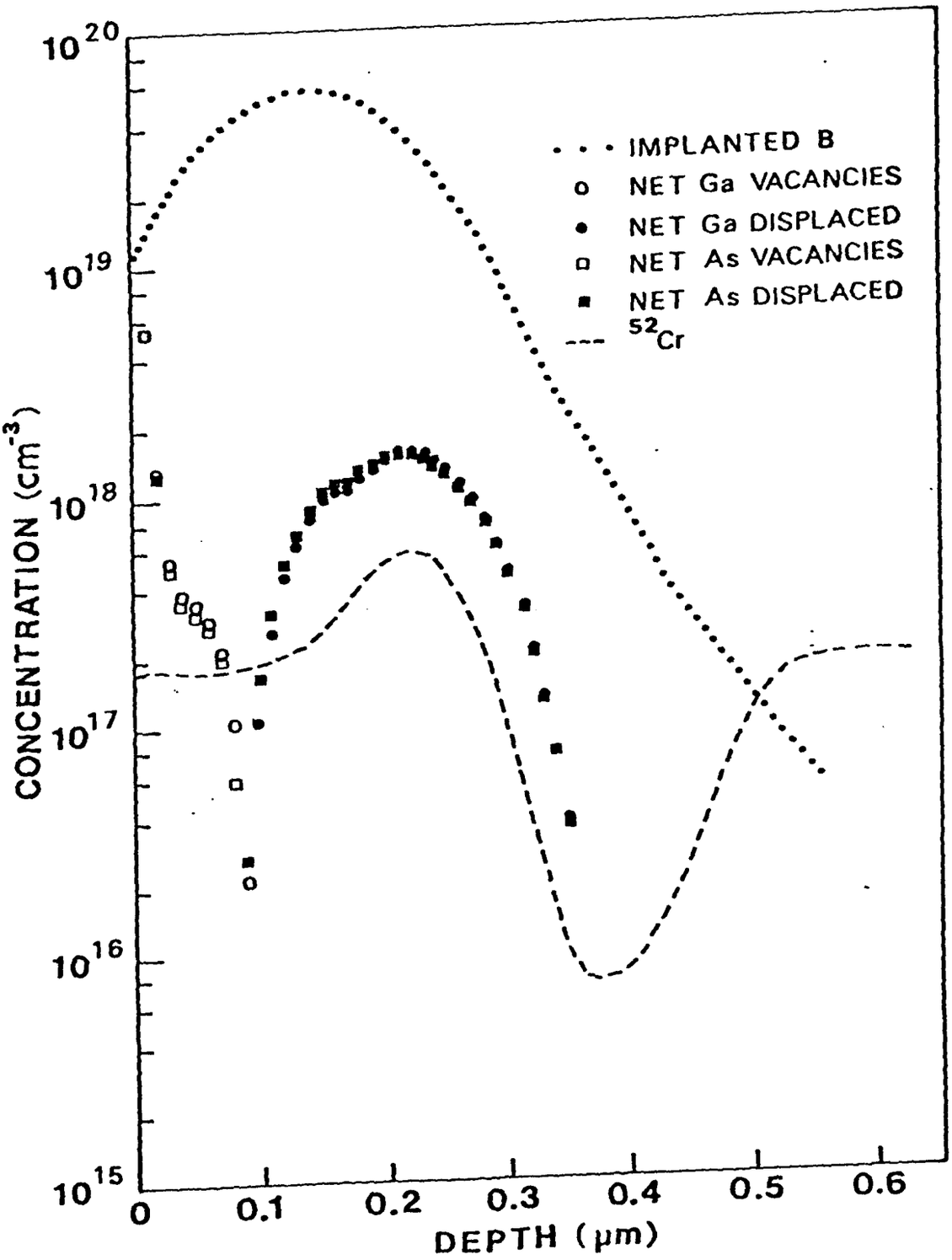

FIG. 6. NET Ga/As VACANCIES, NET Ga/As DISPLACED AND Cr REDISTRIBUTION PROFILE IN 500°C, ANNEALED, 50 KeV B-IMPLANTED GaAs SAMPLE.

Based on the current experiments, we observe a definite correlation between the Christel-Gibbons model and the observed Cr redistribution. Further work is required, however, to assess the influences of predicted stoichiometric disturbances on Cr redistribution in samples implanted with heavier ions (S,Se,Si) to doses known to produce an amorphous layer.

5. FIELD ENHANCED DIFFUSION OF Cr AND CONTACT DEGRADATION IN GaAs FETs

The problem of contact degradation in GaAs FETs has been an area of concern to device manufacturers for the past 10 years. Although numerous investigations have attempted to improve contact alloying procedures, there have been no definitive studies identifying mechanisms responsible for contact failure under thermal-bias stress testing.

Recently, we reported that simple short term alloying of Au contacts on substrates or LPE layers on S.I. substrates produced rapid redistribution and gettering of Cr into damage regions created by the low temperature alloying process. At that time, we suggested that accelerated motion of Cr into alloy zones and diffusion of Cr into interfacial regions might possibly be related to the observed contact failure during thermal-bias stress tests.

To further investigate this problem, GaAs FETs were fabricated by Avantek Inc. using conventional Au-Ge/refractory metal contact alloying on VPE (buffer/active) layers grown on S.I. substrates (Cr-doped).

In Fig. 7 we show an optical micrograph of the FET structure used in these experiments. To provide a systematic evaluation, we devised a series of test configurations for both electrical and impurity profiling tests. Figure 8 shows a matrix description of the tests conducted. The objective of the thermal-stress-bias tests was to determine the relative change in Rs and Rd as a function of stress time and to determine if the previously reported results of selective drain degradation could be related to the motion of Cr in the presence of an electric field.

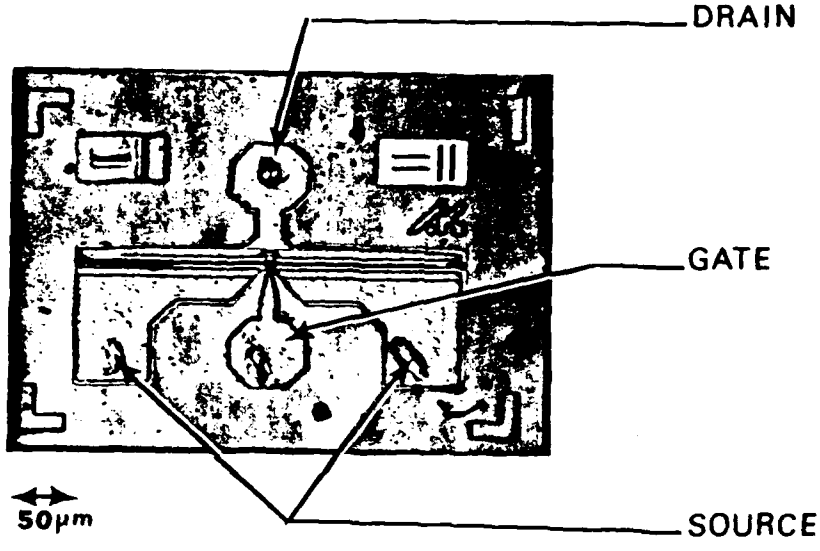

FIG. 7. OPTICAL MICROGRAPH OF FET TEST STRUCTURE.

TEST MATRIX & STRESS CONDITION

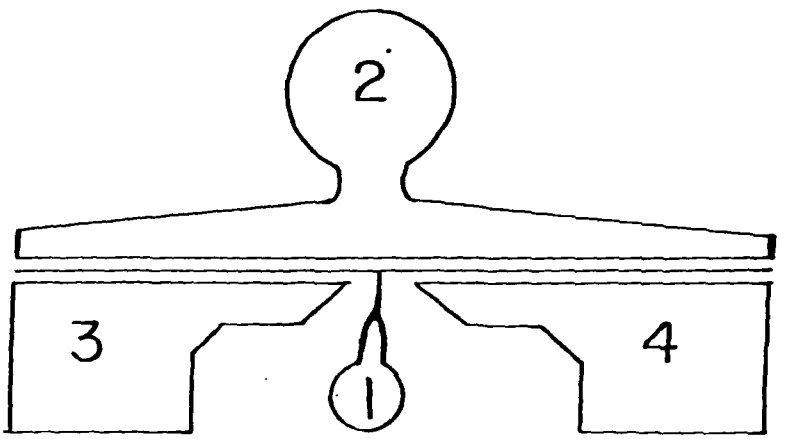

	Drain	Source	Gate	Not connected
Standard	2	3, 4	1	NA
Case 1	3, 4	2	1	NA
Case 2	4	2	1	3

	V_{ds}(V)	I_{ds}(mA)
Standard A	3	10
Standard B	3	20
Standard C	5	10
Standard D	0	0
Case 1	3	10
Case 2	3	5

FIG. 8. TEST MATRIX FOR ACCELERATED STRESS-BIAS TESTS.

In Fig. 9, we show Cr concentration profiles in depth obtained within the drain contact region after alloying and after subsequent annealing at 270°C for 161 hrs. (no bias). In both the source and drain contact regions, we observe a significant gettering of Cr, both within alloy damage regions and slightly deeper into the VPE layer. This motion and gettering of Cr into near-surface regions occurs during contact alloying, in agreement with our earlier reported results on modeled contact structures. After annealing for 161 hrs. at 270°C following contact alloying, we observe no significant alteration in the concentration of Cr within the near surface regions. These results are consistent for both drain and source contacts, showing that no further redistribution of Cr occurs (after alloying) during extended low temperature annealing.

In Fig. 10, we show the Cr redistribution profiles obtained from an FET within source and drain contacts after thermal bias stress (5V,10mA;270°C). After 116 hrs. of stress, we detect essentially identical distributions of Cr under the source contact as observed after alloying, in agreement with the data shown in Fig. 9. Under the drain contact, however, we observe significant diffusion and pileup of Cr at the metallization/GaAs interface. Increased motion and pileup of Cr occurs as a function of increasing stress time.

The results show that Cr diffuses under the drain region producing a region (1000Å to 2000 Å thick) near the surface containing high concentrations of Cr ($>10^{20}/cm^3$). In the source region, there is no pronounced diffusion of Cr to the surface and the Cr concentration remains the same as observed after contact alloying.

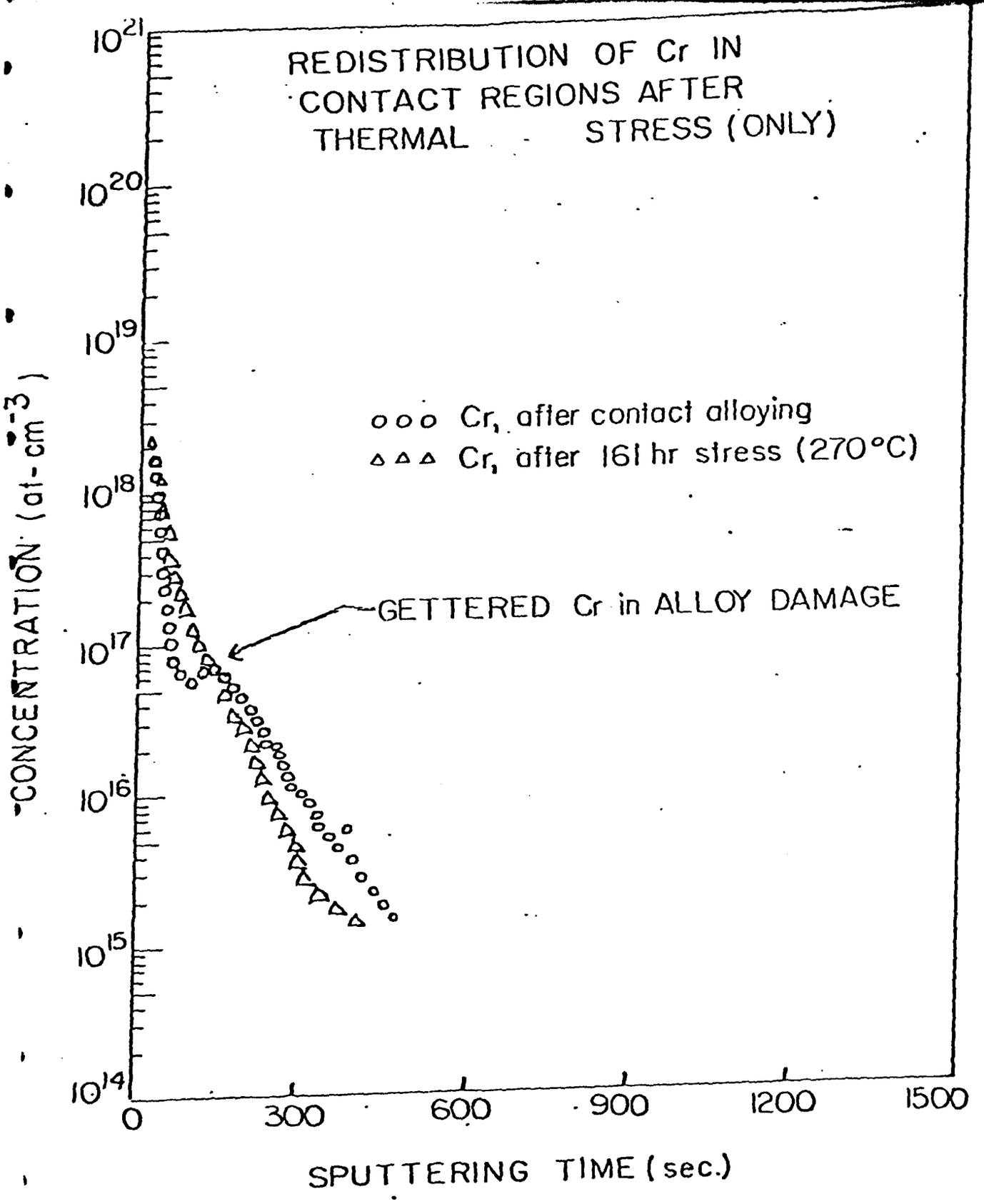

FIG. 9. CHROMIUM REDISTRIBUTION PROFILES IN DEVICES SUBJECTED TO THERMAL STRESS (ONLY)

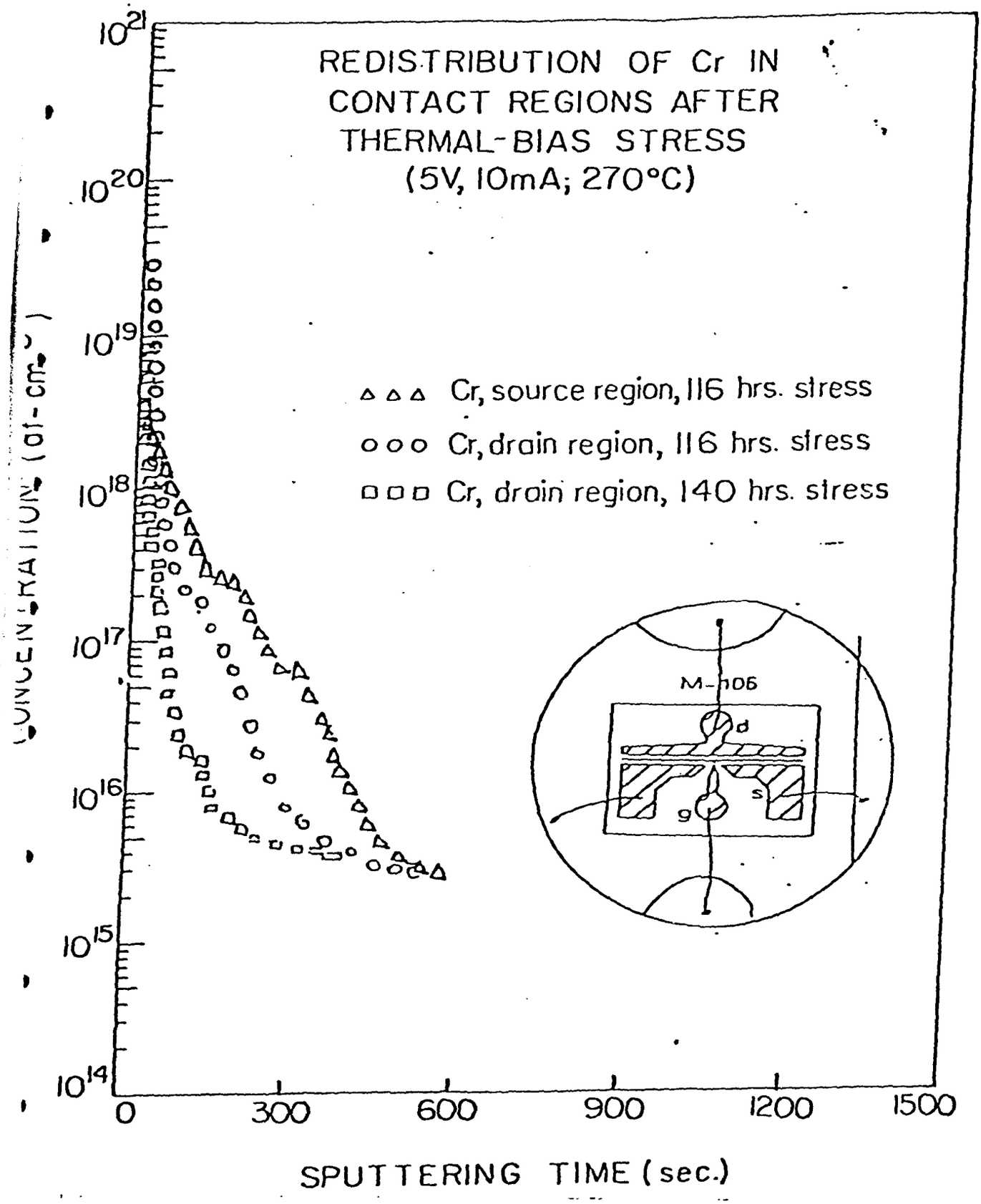

FIG. 10. CHROMIUM REDISTRIBUTION PROFILES IN CONTACT REGIONS AFTER THERMAL-BIAS STRESS (5V, 10mA; 270°C) FOR VARIABLE PERIODS.

Figure 11, shows Cr redistribution profile under source and drain contacts after thermal-bias stress under reduced voltage-bias conditions (3V,20mA;270°C). We observe a similar pattern of diffusion under the drain contact, while the source region shows no prominent redistribution of Cr after stress testing. Of interest, however, is the fact that the displacement of the Cr diffusion front is reduced relative to results obtained at 5V for comparable stress periods. These results suggest that the diffusion and pileup of Cr at the surface is directly proportional to the magnitude of the applied voltage.

To further evaluate the effect of voltage bias on Cr diffusion we performed a similar series of experiments in which the voltage remained constant and the input current was varied in a second series of tests, the current was held constant and the voltage increased in separate experiments. The results showed that the amount of Cr diffusing to the surface under the drain contact was influenced predominantly by the magnitude of the applied voltage. Changes in current did not produce any significant alterations in the pattern of Cr motion, verifying that voltage is the important factor in the enhanced diffusion of Cr.

To provide further confirmation of the field-enhanced diffusion of Cr in contact regions we reversed the polarity on source and drain regions (Fig. 12) and performed additional stress tests. (In the figure we have labeled source and drain regions in their normal configurations). The results show in dramatic fashion the polarity dependent diffusion effect, where the Cr pileup now occurs within the (initial) source region. Also shown for reference is the Cr redistribution on the unbiased (control) contact. It can be observed that no Cr redistribution can be detected and the observed profile is essentially identical to that obtained immediately after alloying.

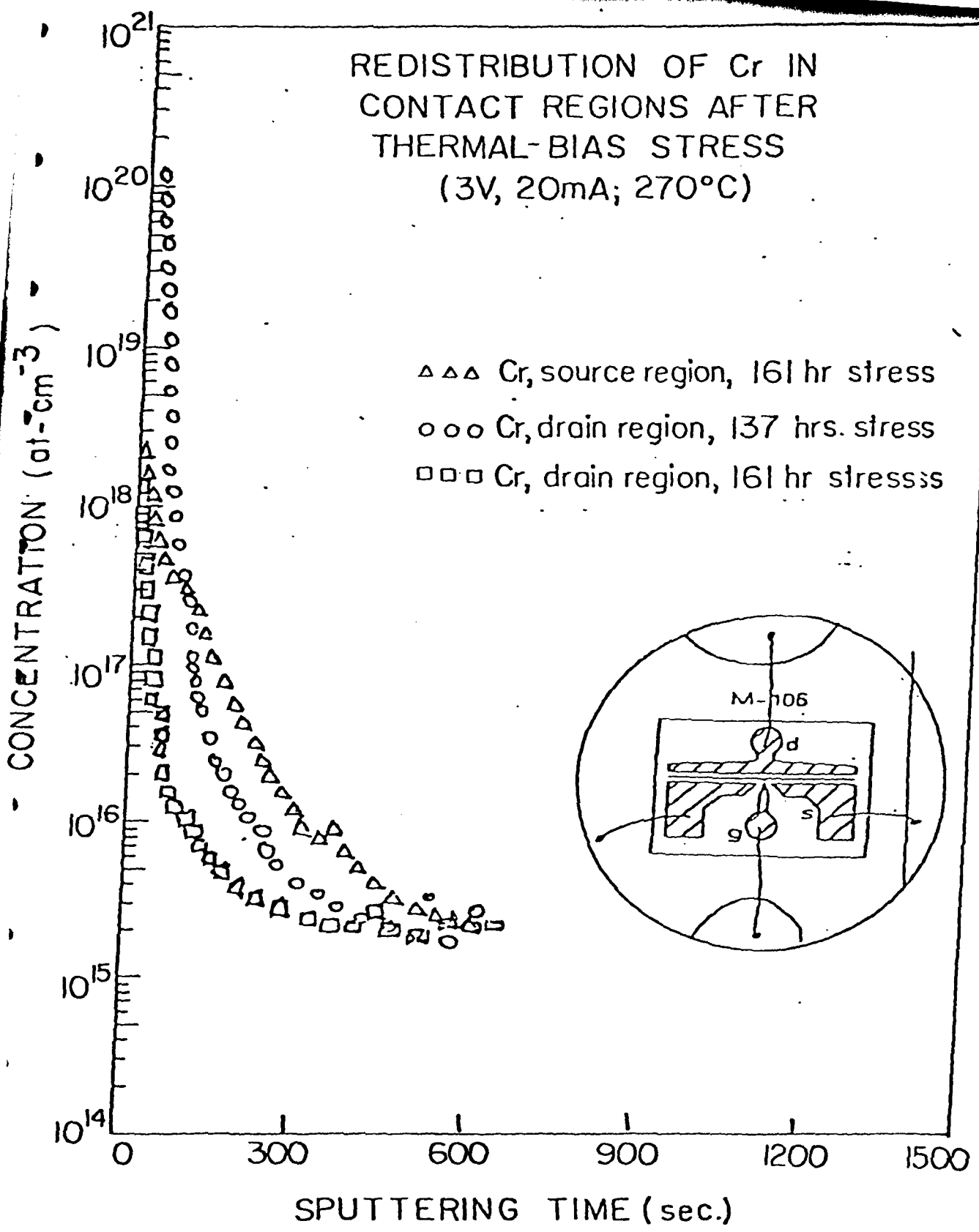

FIG. 11. CHROMIUM REDISTRIBUTION PROFILES IN CONTACT REGIONS AFTER THERMAL-BIAS STRESS (3V, 20mA; 270°C) FOR VARIABLE PERIODS.

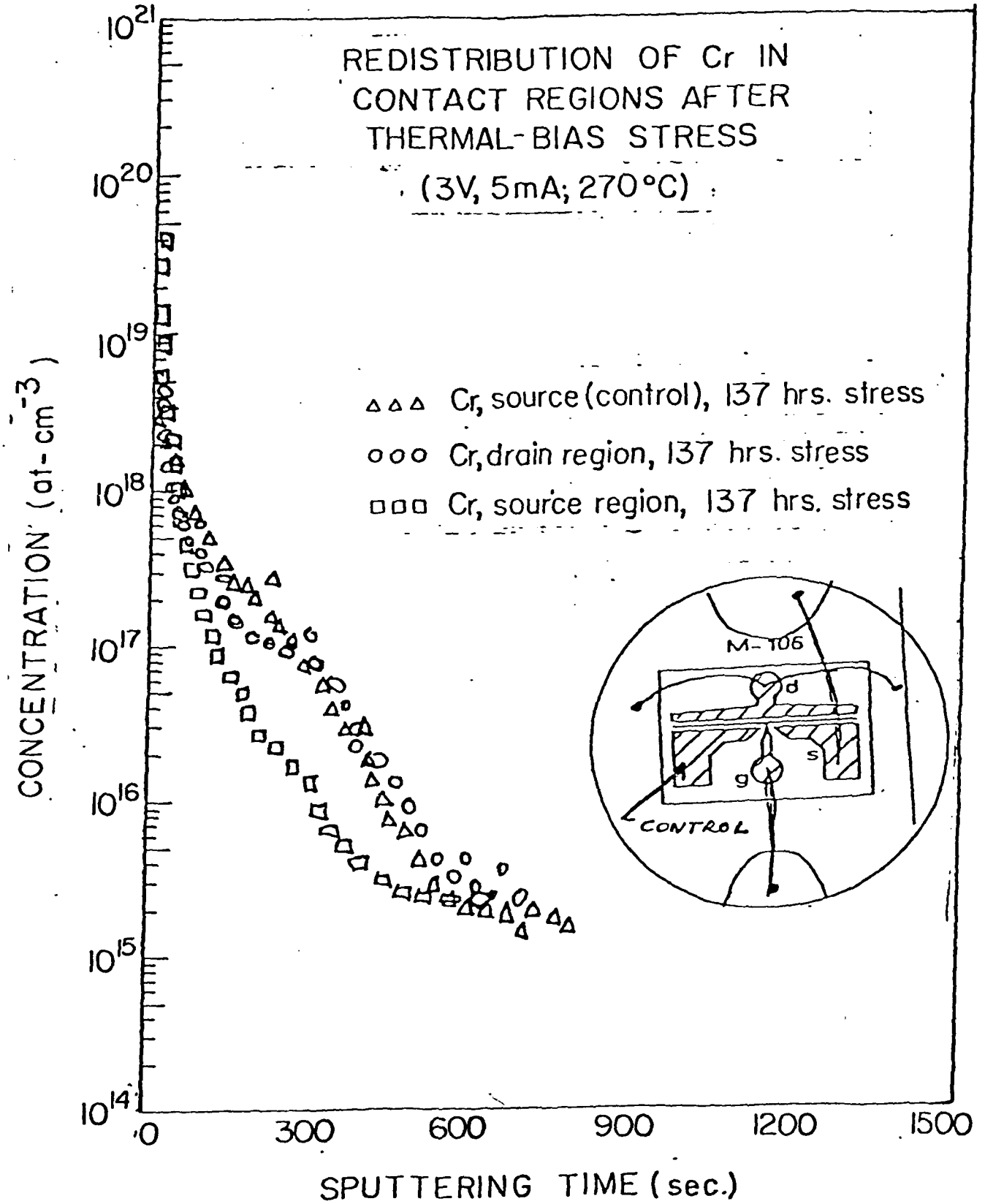

FIG. 12. CHROMIUM REDISTRIBUTION PROFILES IN CONTACT REGIONS AFTER THERMAL-BIAS STRESS (3V, 5mA; 270°C) FOR VARIABLE PERIODS

In Tables 1 and 2, we show representative data obtained on FETs subjected to stress-bias tests for varying times at 270°C. Also included for reference are average R_d and R_s values for devices subjected to thermal stress (only) at 300°C for 617 hrs. Devices subjected to thermal stress alone show no significant differences in R_d and R_s values after annealing. In comparison, under thermal-bias stress at 270°C, when V_{ds} = 5V and I_{ds} = 10mA, (Table 1) we observe that the value of $R_d > R_s$ upon completion of the tests. Similarly, in Table 2 for V_{ds} = 3V, I_{ds} = 10mA, we observe a similar pattern of contact degradation, in which the drain resistance always exceeds the source resistance after thermal-bias stress. In an extended series of tests, we have shown that $(R_d/R_s - 1)$ scales both as a function of increasing stress duration and V_{ds}.

From the data obtained, we can conclude that the failure mode in the GaAs FETs can be explained by the field-enhanced migration of Cr into the drain region, resulting in an increase in R_d relative to R_s upon extended stress testing. This failure mechanism has been shown to be applicable to all devices tested and seems to explain all the other GaAs FET long term failure modes reported by other workers.

The present results indicate that failure will occur even at Cr concentrations as low as $10^{15}/cm^3$. Additional tests are currently required to obtain comparative data on ion implanted source and drain regions within LEC material of varying Cr concentration. It would also be of interest to develop techniques for controlling the field-enhanced diffusion of both oxygen and chromium in GaAs-based device structures.

3V- 10mA 270°C

I_{dss}(mA)					R_s / R_d		$R_d/R_s - 1.00$ (%) $t = t_1$
t = 0	50 hr.	137	161	Δ	t_0	t_1	
42	34			8	5.4/5.0	6.0/6.8	
42	36			6	5.3/4.6	6.4/6.4	6.5
44	35			9	5.1/5.1	6.0/6.4	
44		28		16	5.0/5.0	6.5/7.4	
41		16		25	4.8/5.0	6.4/7.4	17.3
48		24		24	5.0/5.0	6.2/7.6	
43			14	29	5.0/4.9	NA	
48			28	20	5.5/4.8	NA	
40			17	23	5.0/5.0	NA	

TABLE I. DEVICE DATA (3V, 10mA; 270°C)

5V - 10mA 270°C

	I_{dss} (mA)					R_s / R_d		$R_d / R_{s(t=t_1)}$ (%)
	t = 0	46(hrs.)	116	140	Δ	t_0	t_1	
	44		16		28/64	4.5/6.0	6.2/10	
	44		19		25/57	5.2/5.0	6.2/8.4	
	47	32			15/32	5.1/5.0	6.4/5.8	
	32			6	26/81	5.8/5.5	NA	AV. = 31.5
	40	27			13/48	5.2/5.6	6.0/7.2	
	43			8	35/81	5.0/5.5	NA	
	t=0		137	161				
no bias	26		16	-	10/38	6.6/6.2	7.4/7.6	
	42		30	-	12/29	5/5.2	7.4/6.2	

Previous Device Runs

t=0	t=617 hr.	T(°C)	Vds	Ids
R_5 AV. 4.6	6.8	300	0	0
R_d AV. 4.0	6.7			
t=0	t=193 hr.	T(°C)	Vds	Ids
R_5 AV. 5.4	7.1	270	3	10
R_d AV. 4.9	12.3			

TABLE II. DEVICE DATA: BIASED AND UNBIASED, Ts = 270°C; Ts = 300°C

6. SOLUBILITY AND DIFFUSIVITY OF Cr IN GaAs

Semi-insulating wafers of Cr-doped GaAs are used extensively as substrates for the growth of active layers of GaAs by liquid or vapor techniques. The presence of Cr is believed to introduce deep levels in the band-gap which compensate residual impurities, leading to the semi-insulating properties.

In spite of the importance of this topic, relatively little work has been devoted to diffusion and solubility of Cr in GaAs. Two papers by Tuck and co-workers, however, report the results of studies devoted exclusively to the diffusion of Cr in GaAs, using radio-tracer techniques. Two major conclusions were found: diffusion profiles may not be represented by a simple error function solution, and diffusion coefficients are suprisingly large. The results indicate that Cr diffusion in GaAs may be a complicated process, perhaps with both interstitial and substitutional species playing a significant role.

To address these areas, a study of the solubility and diffusivity of Cr in GaAs in experimental systems, in which both diffusion sources and diffusion hosts are well characterized, was initiated. A major consideration is the proper definition of the phase relations in the Ga-As-Cr system and the relationship to diffusion sources of Cr in GaAs. The following three areas are emphasized in the study: phase relations in the Ga-As-Cr system, (with particular reference to establishing regions of co-existence of three phases); determination of the solubility of Cr in GaAs as a function of Cr source and the state of the GaAs host (eg. solute concentration and defect structure); and the diffusion of Cr in GaAs in a Cr concentration gradient, (with particular attention to careful definition of both to diffusion source and the GaAs host.)

Possible isothermal ternary sections can be predicted if three binary temperature-composition phase diagrams are known. Our approach is to establish, to the best of our ability based on previous work and our own work the respective binary systems. With this information, we can predict a few possible isothermal ternary sections. We then wish to establish which of these possibilities is correct by performing phase studies for a relatively few compositions. (The actual type of ternary section will depend on which binary compounds are the dominent ones.)

Once the general pattern of the ternary section is established, the overall composition of three phase regions will be established. Both defferential thermal analysis (DTA) and X-ray diffraction (XRD) techniques will be used in this study. We have carefully studied the original articles describing the Ga-As, Ga-Cr and Cr-As systems. The first two systems have been studied rather extensively, however, there are regions in the Cr-As system, particularly at higher As compositions, that are not reliably known.

To confirm previous work in the Ga-Cr system, we performed DTA on 68.83 a/o Ga - balance Cr and obtained a liquidus temperature within 4°C of that previously reported. We then devoted our efforts to the As-Cr system.

Because of its toxicity and high vapor pressure, As requires particular care in handling. Rather than mixing different ratios of elemental As and Cr to perform DTA measurements, we chose a different approach: the formation of the compound CrAs at lower temperatures (500°C) by a long anneal, and then the addition of either As or Cr to this compound to obtain the desired compositions. Since CrAs has a much lower vapor pressure than elemental As, the risk of a violent explosion during DTA is reduced using this technique. A mixture of

30 gm As and /Cr in a 50-50 atomic ratio was sealed in a quartz ampule and heated to 500°C. However, after one day at this temperature, a small crack formed in the ampule, and fumes were escaping. Some compound formation was evident in the ampule, and this material was examined using an X-ray diffractometer. Diffraction peaks were found corresponding to both CrAs and Cr_4As_3, indicating that this material was this two-phase region. This is reasonable, since one would expect selective loss of As because of its higher vapor pressure. Several anomolous peaks also appeared in the diffraction pattern which cannot be indexed using existing information. Because of the difficulty in CrAs synthesis and because it is commercially available, we have purchased CrAs powder. We are using this to prepare Cr-As compositions for DTA as well as for Cr sources in solubility and diffusivity studies.

We were aware of potentially troublesome behavior during diffusion annealing due to the development of uneven surfaces on previously polished GaAs. Certainly, the selective vaporization of As at sufficiently high temperatures is to be expected in inert gas and vacuum environments. These problems are often described in the literature; however, there appears to be conflicting information. Malbon et al. for example, report that degradation occurs after a 20-minute anneal at 800°C in argon and that the degradation may be prevented by a suitable addition of As to the vapor ambient. Tuck et al. however, do not mention this problem, even for annealing as high as 1000°C without the intentional addition of excess As. This seems unusual since in the annealing of device structures, silicon nitride or silicon dioxide (or a combination) is customarily used to prevent surface degradation. This method (silicon nitride encapsulation) is not desirable for most diffusion studies, however, because it does not allow for well defined external sources of Cr or As.

To study surface decomposition of GaAs wafers under various conditions, several experiments were performed consisting of annealing polished GaAs wafers under well defined conditions and subsequent examination using interference contrast optical microscopy (100-1000X). Si-doped GaAs wafers were sealed in evacuated ampules with no source and annealed at 800°C, 900°C, 1000°C, and 1100°C for two hours each. Each sample was examined for surface degradation; degradation was observed in the samples at 1000°C and 1100°C, whereas the surface appeared unchanged at temperatures under 1000°C. Following these runs, elemental As powder was placed as a source in the sealed ampuled with the GaAs wafers. When the source was reduced to 0.38 atm in a second ampule at 1000°C, it is also showed strong degradation.

Initial diffusion experiments of Cr into GaAs were performed to 1) study effects on surface degradation, 2) compare Cr concentration profiles with previous experiments, and 3) study the effects of using various Cr sources.

In all experiments, the undoped GaAs wafer (1cm x 1cm) was encapsulated in an evacuated quartz ampule, with the source material contained in a bulb at the end of the ampule (3cm from wafer). The ampules were placed in the flat zone of the furnace for the desiganted time and temperature, and then quenched.

In diffusion experiments included the following samples and conditions:

(1) C2: Annealed un-doped GaAs with Cr source, 2 hrs., 1100°C

(2) C1: Annealed un-doped GaAs with Cr source, 2 hrs., 900°C

(3) CA10: Annealed un-doped GaAs with CrAs source, 2 hrs., 1100°C

(4) CA11: Annealed un-doped GaAs with CrAs source, 2 hrs., 900°C

(5) D: As-received undoped GaAs (Crystals Specialties).

The SIMS profiles obtained from samples C1 and C2 are shown in Figs. 13,14 and 15,16 respectively. In most of the profiles, the As concentration decreased over a one micron region at the source to roughly one quarter of the surface concentration, then remains constant. Note also that there is an inflection in the Cr concentration profile at the same depth as the As inflection. There were no SIMS profiles obtained from sample C10 because of experimental problems encountered during the diffusion anneal. The SIMS analysis of the sample CA11 showed a very high and nearly constant Cr concentration profile ($\simeq 10^{19}$), with a small dip at the surface.

The C_o (surface concentration) and C_B (bulk concentration) values compare fairly well with Tuck's results:

	C_o	C_B
Tuck's 900°C 2 hr. (extrapolated from longer times)	1.0×10^{17}	7.0×10^{15}
Our 900°C 2 hr. (C2)	1.0×10^{18}	5.0×10^{15}
Tuck's 1100° 2 hr.	2.4×10^{17}	1.3×10^{16}
Our 1100°C 2 hr. (C1)	8.0×10^{17}	2.0×10^{15}

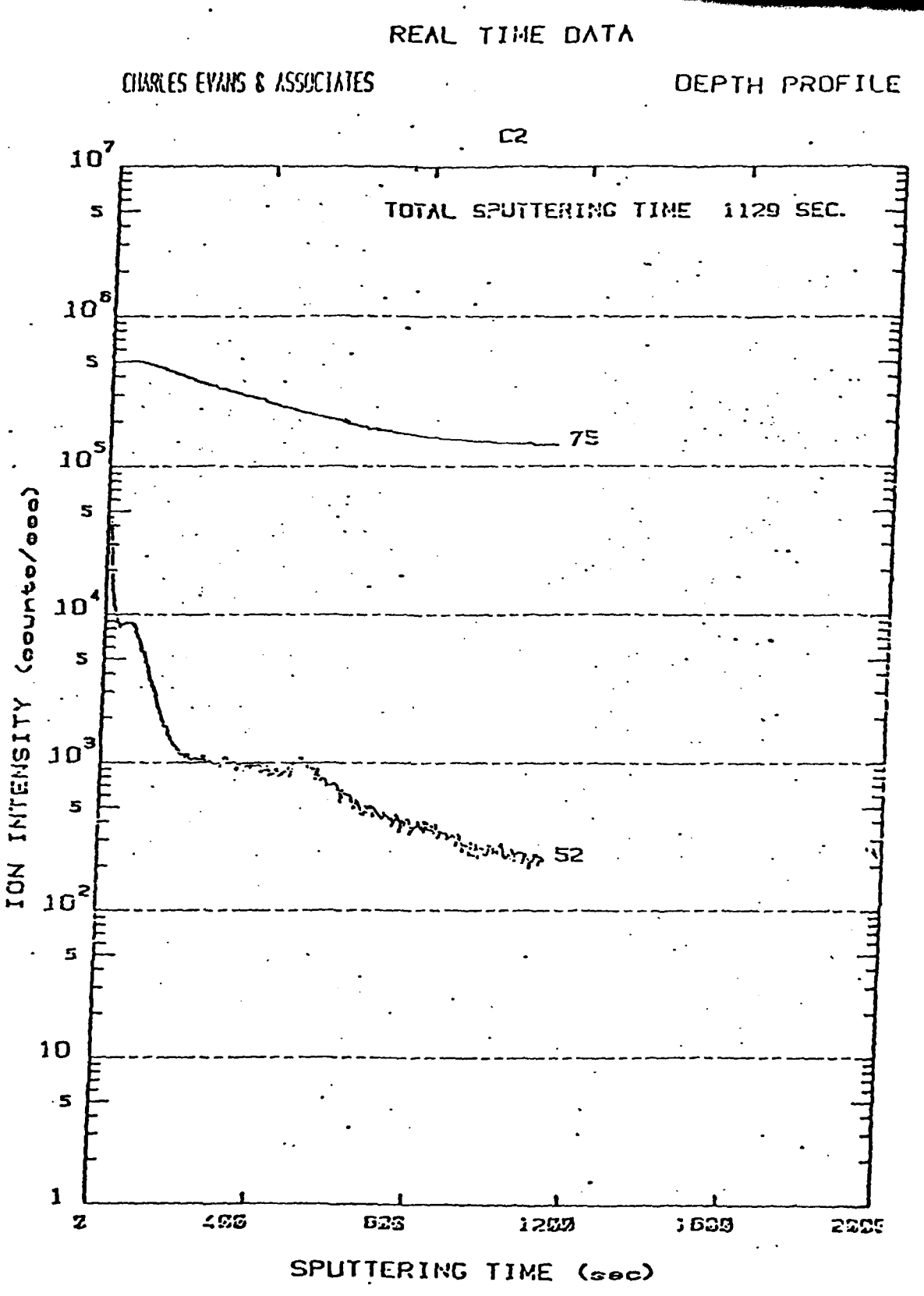

FIG. 13. SIMS (ION INTENSITY) PROFILE OF Cr FOR SAMPLE C2.

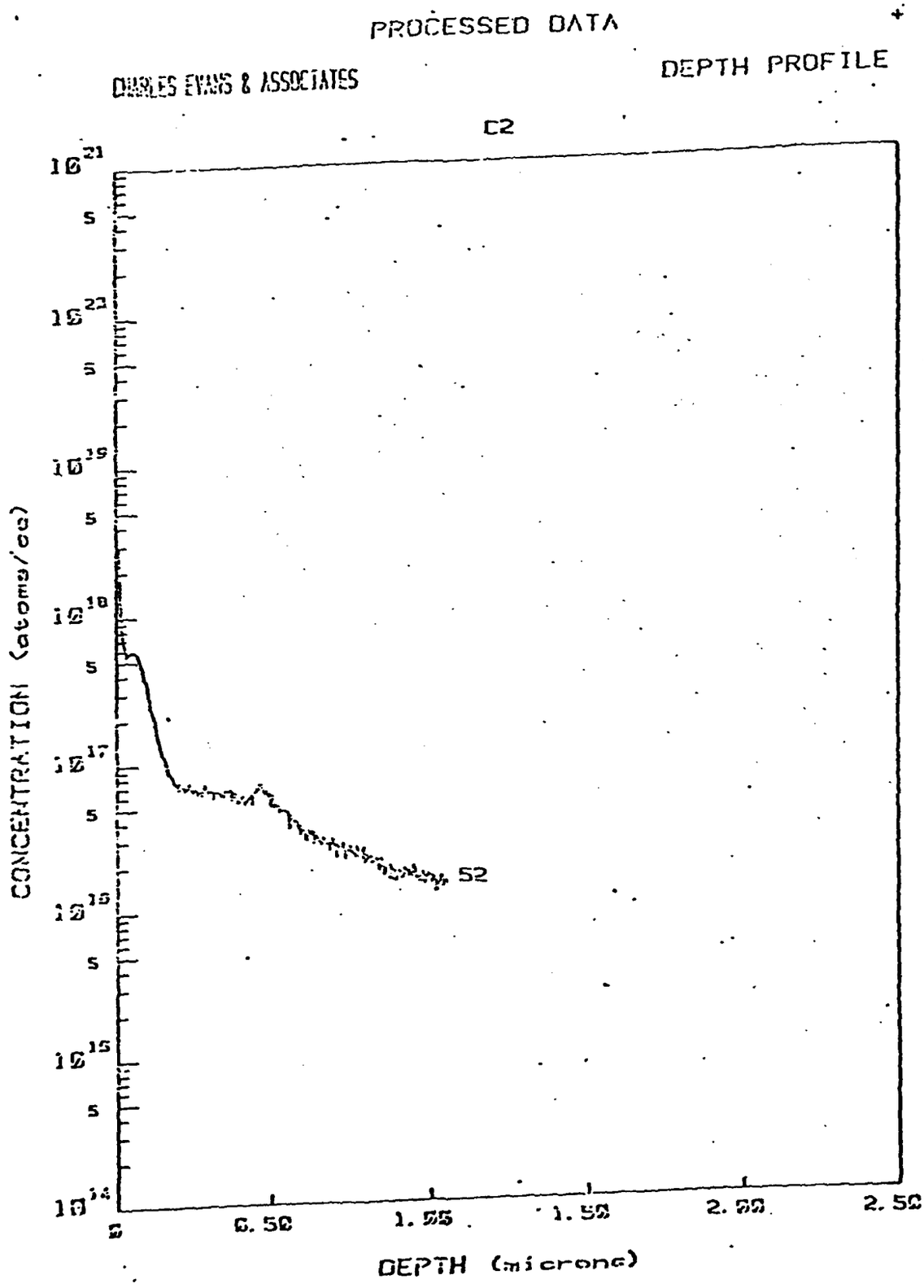

FIG. 14. SIMS CONCENTRATION PROFILE FOR Cr IN SAMPLE C2.

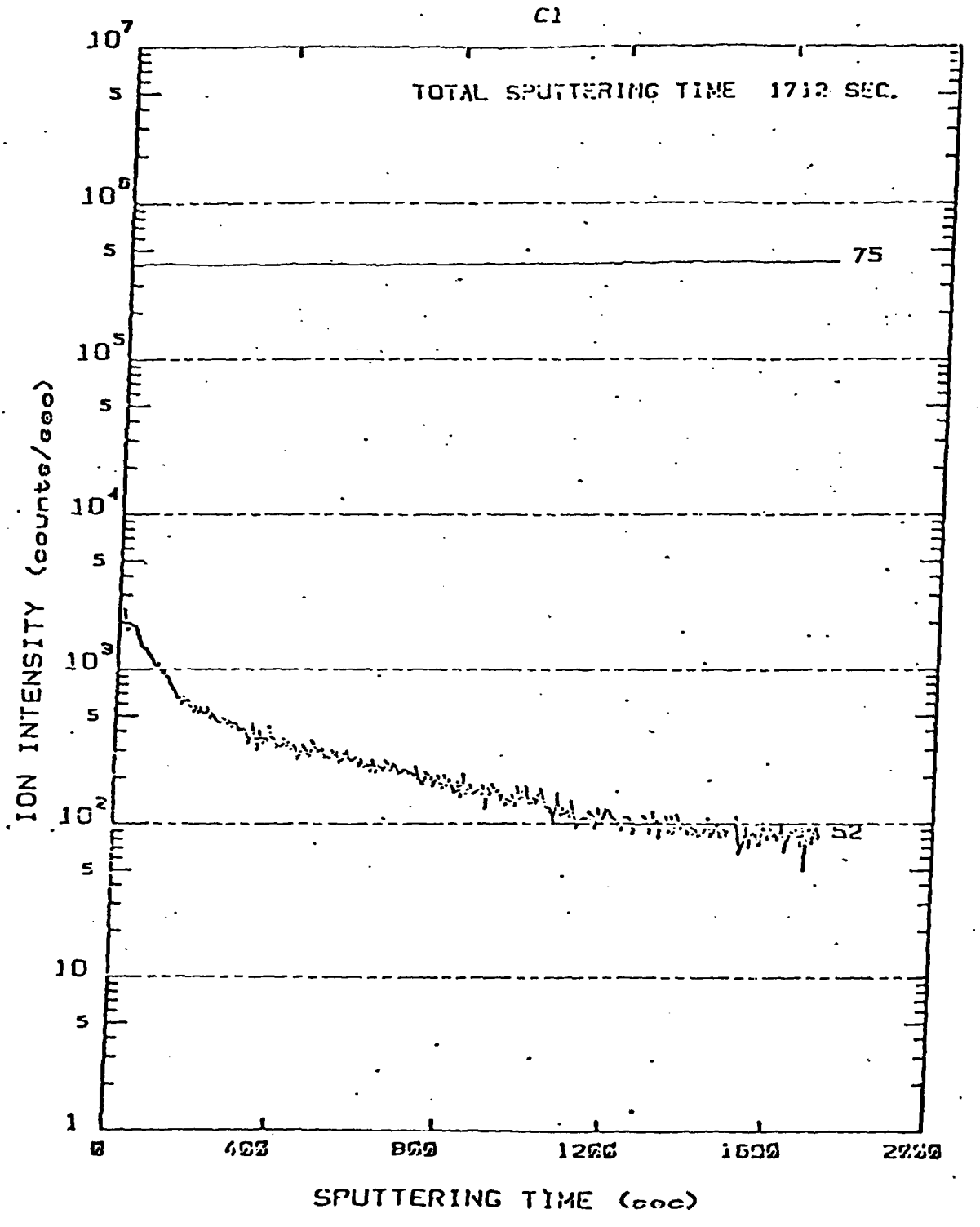

FIG. 15. SIMS (ION INTENSITY) PROFILE OF Cr FOR SAMPLE C1.

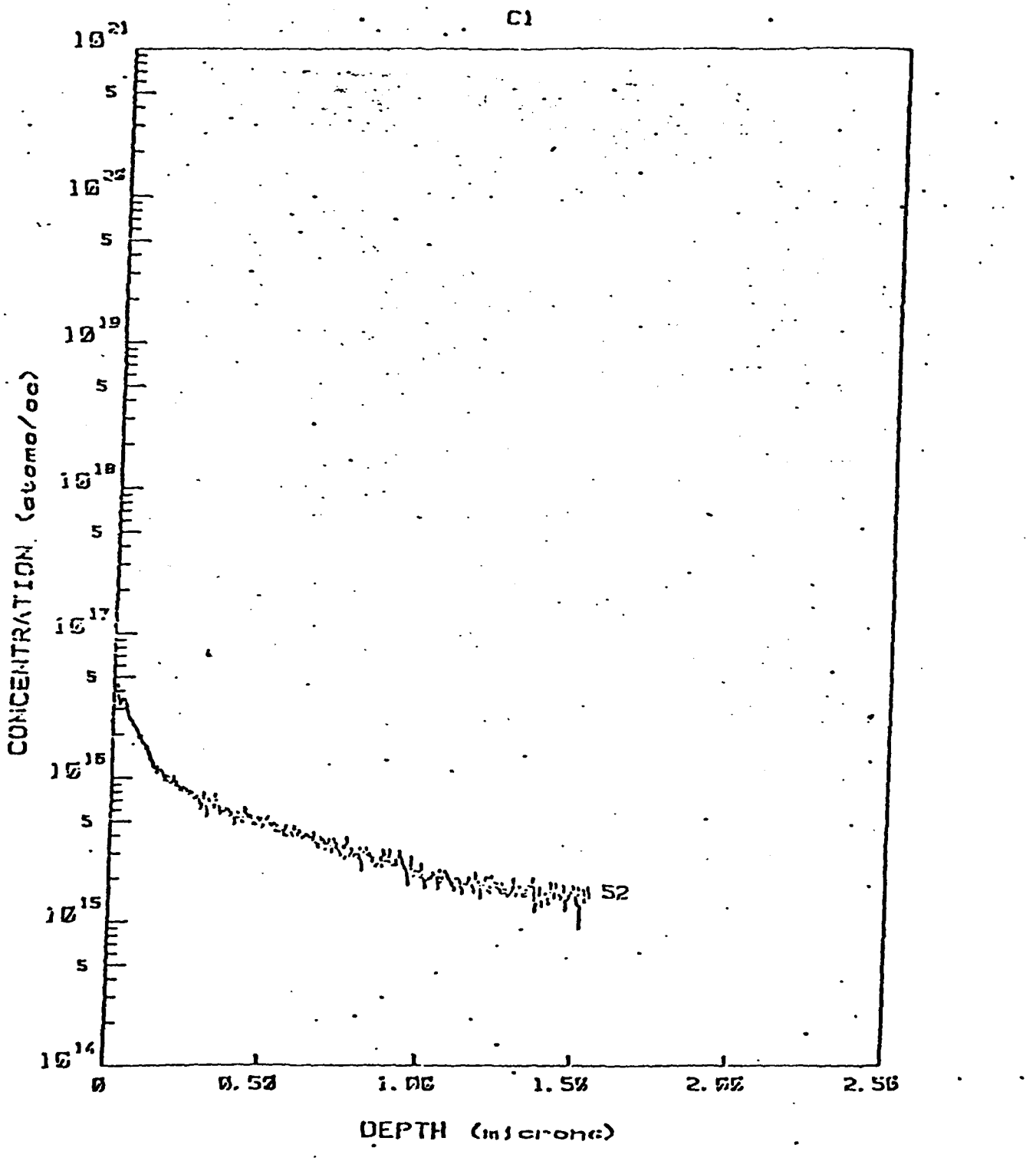

FIG. 16. SIMS CONCENTRATION PROFILE FOR Cr IN SAMPLE C1.

A major difference from Tuck's data is that in our profiles, the decrease from surface to bulk levels occurs much sooner (drop-off depth ≈ 1 micron), while in Tuck's data, the depth at which this decrease occurs is about 20 microns.

The As concentration change in sample C2 (900°C anneal) indicated non-stoichiometry of GaAs at the surface. This does not occur in the 1100°C anneal sample, except on the backside in which it occurs within about 0.5 μm from the surface. Tuck and Khludkov would not have seen this since they did not measure the As concentration. In addition, Magee and Kasahara might not have seen this because they only worked in the 800°C range and below.

Some of Tuck's profiles also show a inflection or a "bump" in the transisiton region from surface to bulk. Further investigation of this inflection, implies a coupling between the Cr and As profiles.

The very high Cr concentration of #CA11 (900°, CrAs source) and the coalescence of #CA10 with the source (1100°, CrAs source) is probably related to phase reactions in the Cr-As-Ga system. This emphasizes the importance of more ternary phase equilibria information. This ternary system is presently being studied in more detail.

Recent literature concerning the three binary systems (Cr-Ga, Cr-As, and GaAs) has provided us with enough information (i.e., stable binary compounds at various temperatures) to propose tentative isothermal sections for the Ga-As-Cr ternary. We will first experimentally determine the X-ray diffraction patterns of two binary compounds (CrGa and $CrGa_4$), for which patterns are not yet available. (We have the patterns for the other eleven binary species).

We will then experimentally determine the pseudo-binary tie lines of the Ga-As-Cr system, by mixing the relevant compositions, followed by an anneal and quench. Subsequently, we will obtain x-ray diffraction data for identification.

We will continue the out-diffusion experiments (depending on the results of the experiments mentioned earlier). Using the two-zone furnace, the Ga/Ga_2O_3 source may be at different temperatures so that the pressure of oxygen can be varied.

7. DEFECTS IN CdTe,HgCdTe, AND LPE-HgCdTe/CdTe

Although a significant amount of research has been reported over the past decade on the growth of HgCdTe, a considerable number of problems remain yet to be solved. Of particular importance is the control of LPE growth of HgCdTe on CdTe substrates. Recent problems in device yield and performance have underscored the need for increased understanding and control of processing procedures.

A number of programs have recently emphasized the need for improved quality of starting CdTe substrate materials. In our initial investigations of the quality of CdTe material available from manufacturers, we observed extreme variability in the concentration of microstructural defects in wafers supplied. In Figs. 17-19, we show representative bright-field transmission electron micrographs obtained from typical CdTe substrates. Although several DoD sponsored programs have claimed to have improved the quality of CdTe, evaluations of this material shows that no substantial improvements have in fact been attained.

The quality of epitaxial layers grown on CdTe material is critically dependent on the interfacial defect density, as is the case for any epitaxially grown layer. In Fig. 20, we show a typical interfacial defect structure within the LPE-HgCdTe layer, generated at a step on the CdTe surface. Within the LPE layers we also observe stacking faults (Fig. 21) and large concentrations of dislocation lines (10^7 to $10^9/cm^2$) in the form of nested arrays (Fig. 22). Unfortunately, such defects are routinely observed in IR detector material. Lateral variations in defect concentration are especially prevalent in commercial material, producing problems in fabrication and yield.

FIG. 17. BRIGHT-FIELD TRANSMISSION ELECTRON MICROGRAPH OBTAINED FROM CdTe SUBSTRATE SHOWING PRESENCE OF DISLOCATION LINES AND LOOPS.

FIG. 18. BRIGHT-FIELD TRANSMISSION ELECTRON MICROGRAPH OBTAINED FROM CdTe SAMPLE SHOWING DISLOCATION NESTING.

CdTe SUBSTRATES

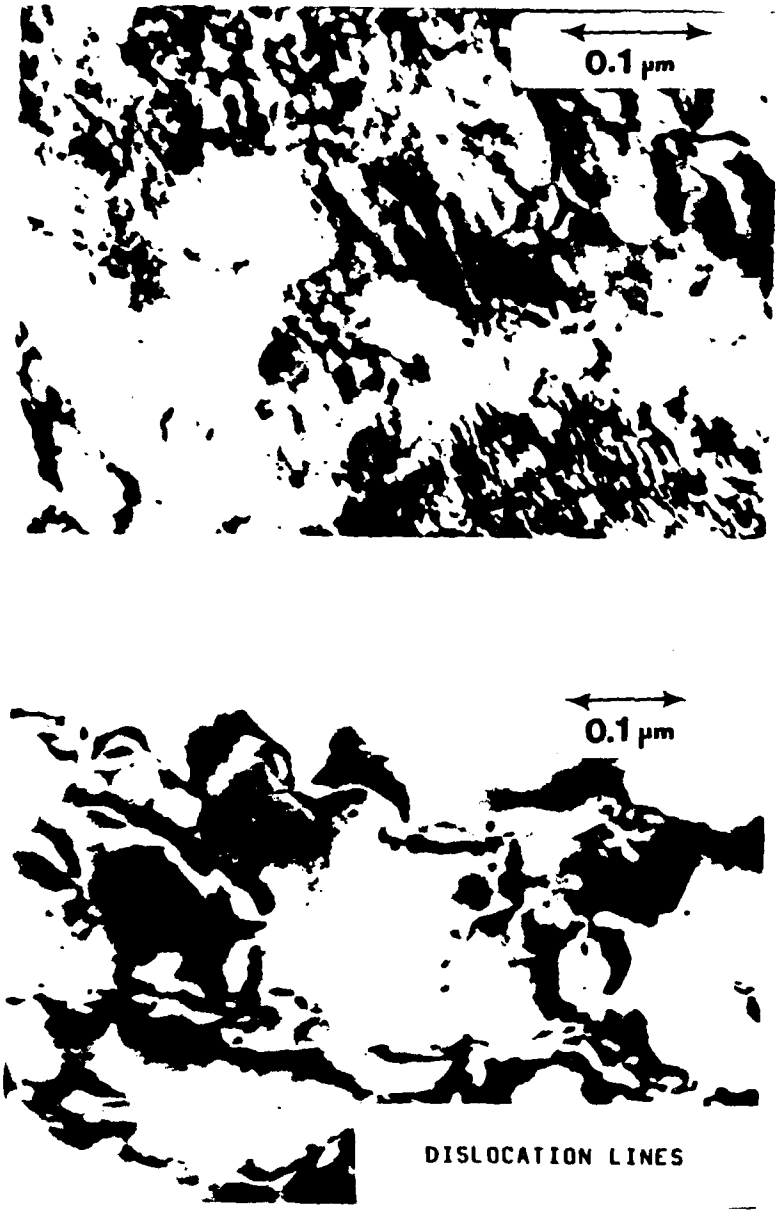

FIG. 19. BRIGHT-FIELD TRANSMISSION ELECTRON MICROGRAPHS OBTAINED FROM CdTe SUBSTRATE SHOWING EXTENSIVE DISLOCATION NESTING.

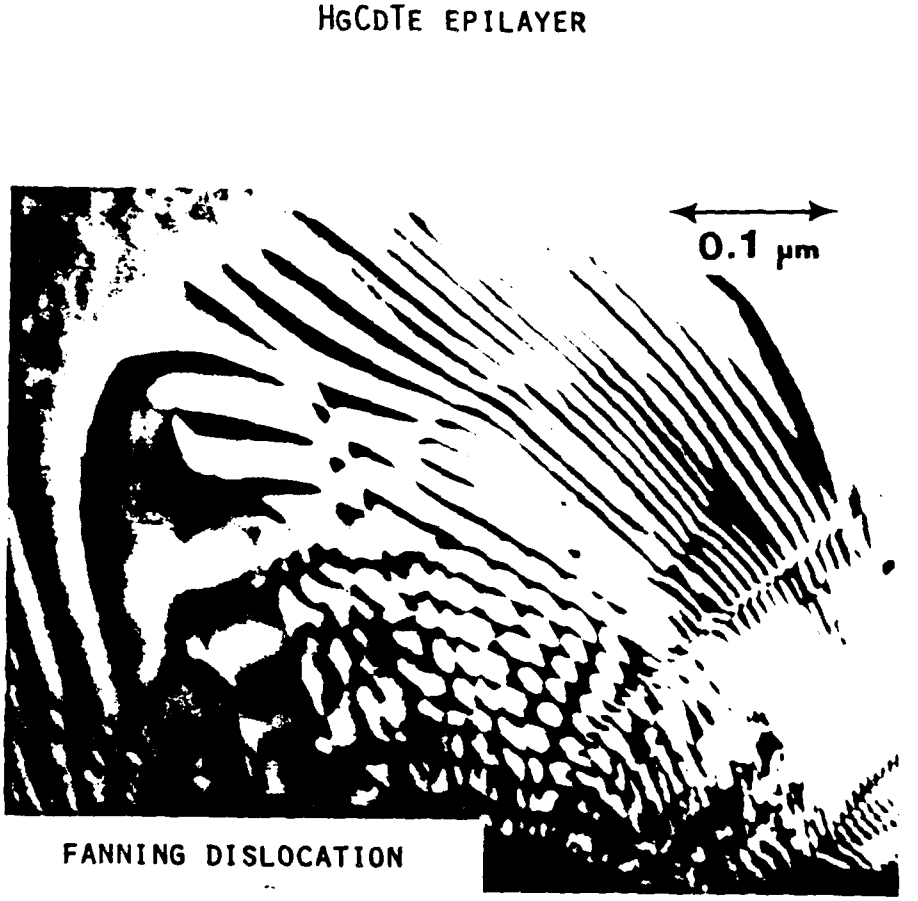

FIG. 20. BRIGHT-FIELD ELECTRON MICROGRAPH SHOWING FANNING DISLOCATIONS IN HCT EPILAYER AT SUBSTRATE STEP.

FIG. 21. BRIGHT-FIELD ELECTRON MICROGRAPH SHOWING PRESENCE OF DISLOCATION LINES LACING STACKING FAULTS IN HCT EPILAYER.

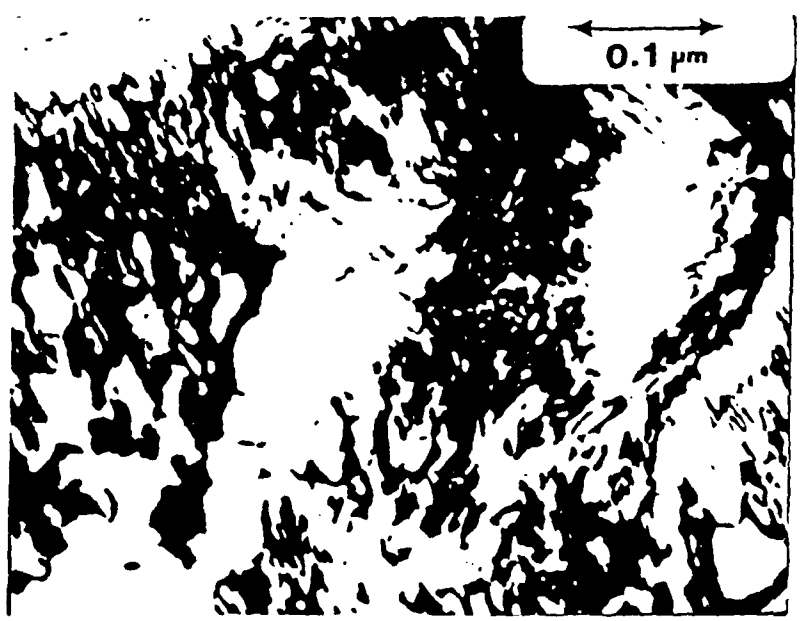

FIG. 22. BRIGHT-FIELD ELECTRON MICROGRAPH SHOWING PRESENCE OF HEAVY DISLOCATION LINE NESTING IN HCT EPILAYER.

The presence of defects within the CdTe and LPE interfacial layer has been shown to result in rapid diffusion of impurities from the substrate and gettering within the interfacial defect region. Secondary ion mass spectrometry profiling shows rapid mobility of In and other impurities into the LPE layer.

To address this problem requires that the defect concentrations be reduced below current levels observed in CdTe substrates. During the past few months, we have begun initial experiments on developing gettering procedures for CdTe substrates. Preliminary results are encouraging and indicate that the technique should be successful. Further tests are now required to evaluate improvements in epitaxial layers grown on the pre-gettered materials. Discussions with TI researchers have also indicated that the control of outdiffusing impurities will be on especially important factor, particularly for second generation devices.

A second problem area we have observed in the production of IR detectors is the lack of critical control of substrate alignment, prior to cutting and polishing. Although x-ray diffraction is normally used, the procedures normally do not permit accurate multi-axis orientation. As a result, the quality of LPE films varies from run to run and yield suffers accordingly. In the extreme, this problem is readily observed in the occurrence of steps at the substrate surface that subsequently appear as deformations at the surface of the LPE layer. At each step site dislocation lines are generated and extend to the surface of the film.

It would be advantageous to provide automated crystal alignment procedures to guarantee multi-axis orientation

within ± 30 sec. of are (reproducibly). This is not currently possible for routine production line procedures. However, there is a technique that is adaptable to CdTe for detector applications (using technology developed under DoD funding) that permits computer-controlled alignment to ± 10 sec. of arc, requiring approximately a 40 second time duration.

Using U.S. Army funding (Fort Monmouth,N.J.), ARACOR is developing a system for aligning quartz crystals within ± 10 sec. of arc. The system utilizes an x-ray source and multiple detectors mounted above a gimballed stage. Using developed algorithms, the diffracted intensities are sampled and inputed to provide precise stage positioning within preprogrammed limits. This system is currently operational but has not yet been applied to CdTe crystal alignment for detector applications. Evaluation is currently required to determine the applicability to CdTe crystals.

In evaluations of both bulk and LPE HgCdTe, we have found that internal (localized) variations in stoichiometry can result in defect nucleation apart from extrinsic sources. However, in cooperative work with Maurice Brau (TI) it has been shown that careful control of stoichiometry and growth in a slight Hg excess can produce crystals of minimal defect density. In previous annealing experiments, we have shown that low-temperature annealing produces Hg outdiffusion (as anticipated) and results in the nucleation of secondary defect structure extending into the interior from the surface of the material (Fig. 23).

To assess the effect of controlled temperature anneals in an Hg overpressure, we have obtained from TI samples annealed for variable periods. Using the newly developed procedure for cross-sectional TEM analysis of HgCdTe, we have

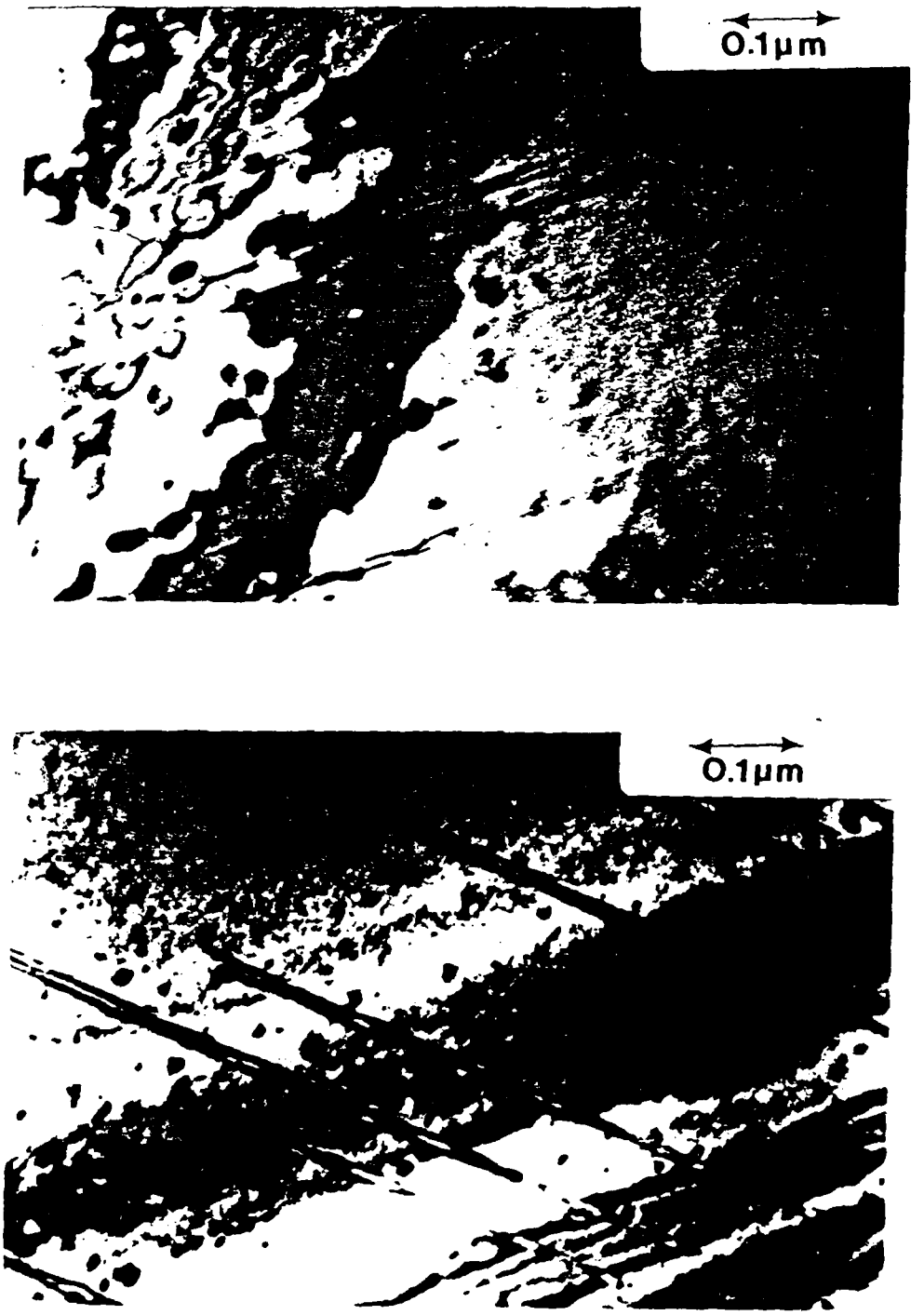

FIG. 23. BRIGHT-FIELD ELECTRON MICROGRAPHS OBTAINED AT SURFACE OF HCT EPILAYER AFTER 1/2 HR., 150°C ANNEALING.

examined defect concentrations as a function of depth from the surface after annealing. Preliminary results indicate a reduction in defect density as a function of increasing distance from the front surface of the sample. Further experiments are continuing to assess the influence of Hg annealing on defect nucleation, but our results indicate that a number of Hg vacancies are not annealed and appear as vacancy loops of varying concentration.

In Fig. 24, we show a transmission electron micrograph obtained in vertical cross at the center of a HgCdTe wafer annealed in Hg vapor for a specified interval at TI. We observe the presence of large concentrations of Te precipitates, dislocation nesting and dislocation loops. When vertical cross-sections are obtained at a depth of 125 μm (from the front surface) we detect no significant dislocation nesting and an apparent absence of Te precipitation as shown in Fig. 25. From those results we can conclude that the controlled anneals in Hg vapor reduce the effective concentration of defects within distances equal to the Hg diffusion depth. In the core region of the dample, excessive Te precipitation and dislocation nesting are detected.

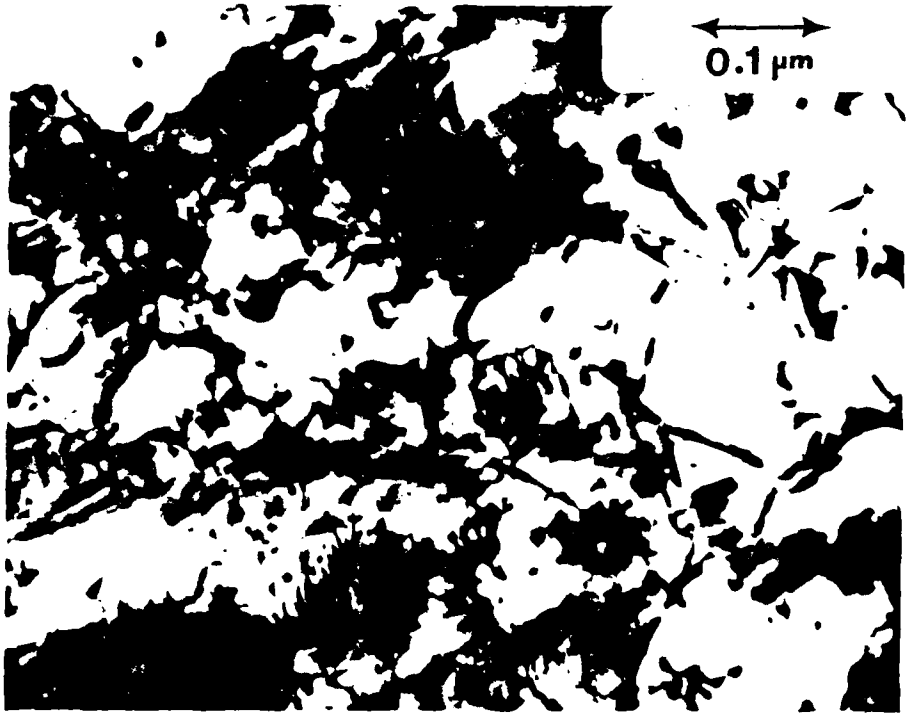

FIG. 24. VERTICAL CROSS SECTION BRIGHT-FIELD ELECTRON MICROGRAPH OBTAINED AT THE CENTER OF HCT (BULK) SAMPLE, SHOWING Te-RICH ZONE AND HIGH CONCENTRATION OF DEFECTS.

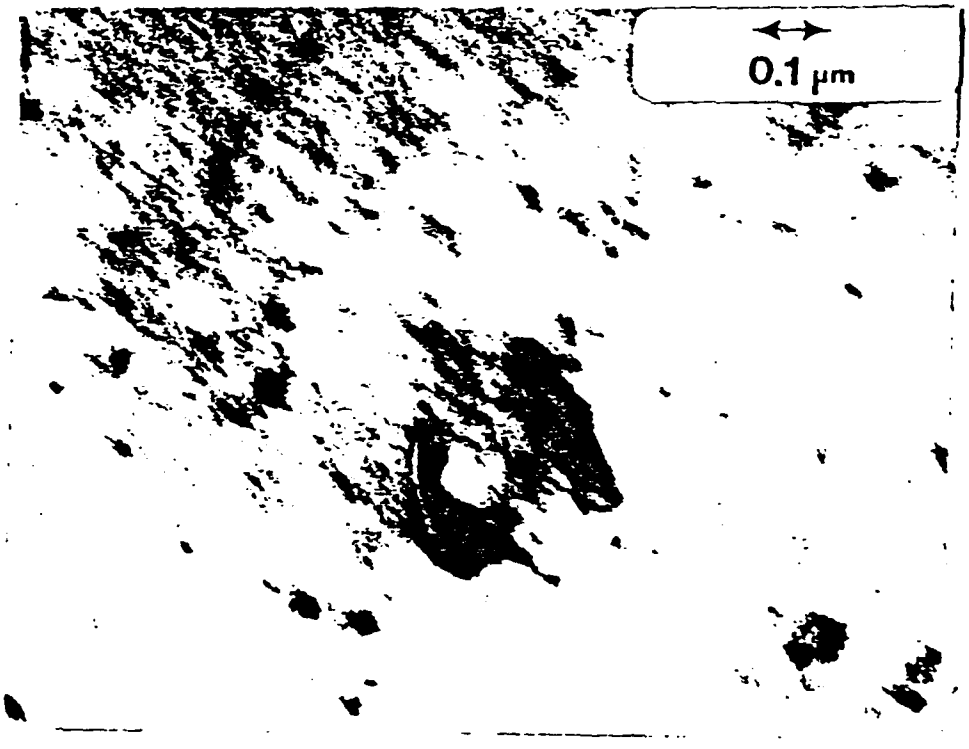

FIG. 25. VERTICAL CROSS SECTION BRIGHT FIELD ELECTRON MICROGRAPH OBTAINED AT DEPTH OF $\simeq 125\,\mu m$ FROM FRONT SURFACE, SHOWING RELATIVE ABSENCE OF DEFECTS.

8. RAPID REDISTRIBUTION AND GETTERING OF OXYGEN IN CZ-Si

As an adjunct to the present program on impurity motion and gettering in semiconductor materials, we decided to use some of the technology and analytical procedures developed for investigating the problem of oxygen mobility in Si.

The role of oxygen in influencing the electrical properties of silicon has received considerable attention over the past ten years. With the increasing demand for more detailed information on impurity redistribution and process-induced alterations to materials properties, the subject of oxygen redistribution in Si has remained an illusive topic and inferences have typically been drawn from bulk infrared absorption measurements on Si wafers. However, such techniques have limited utility in the investigation of localized redistribution of oxygen within regions of importance to device technology. In this section, we present the results of investigations on the rapid diffusion of oxygen into ion implanted (process) regions or defect regions produced by mechanical abrasion at the back surface of a wafer.

8.1 GETTERING OF MOBILE OXYGEN AND DEFECT STABILITY WITHIN BACK SURFACE DAMAGE REGIONS IN Si

In recent investigations[16-20] it has been demonstrated that motion of oxygen toward the center of annealed Czochralski (CZ) Si wafers and subsequent precipitation is effective in producing defects that serve as sites for trapping of impurities in intrinsic gettering procedures. Of equal importance, is the influence of oxygen on damage (thermal) stability in extrinsic gettering. In this paper we present data obtained from secondary ion mass spectrometry (SIMS) profiling, transmission electron microscopy (TEM), secondary ion microscopy, and scanning electron microscopy (SEM) measurements on the role of back surface damage regions in gettering of mobile oxygen and the influence of oxygen precipitation on secondary damage nucleation at the wafer backside.

Samples used in this study were n- and p-type, 75 mm diameter, 400 m thick CZ Si wafers of [100] orientation ($\pm 1°$). Oxygen concentrations in the range, 1.0 to 1.2 x 10^{18} cm^{-3}, were determined by Fourier transform infrared (FTIR) absorption measurements on unannealed wafers using ASTM procedures[21]. Back surface damage was introduced in Si wafers using a rotary abrasion technique [22-24] to create concentric spiral grooves extending to an average depth of $\sim$8 to 10 μm into the surface. Annealing was done either in a flowing N_2 atmosphere or in an oil-free vacuum system at a vacuum level of $\lesssim 10^{-8}$ Torr. In separate experiments, samples were annealed under the following conditions: a) 600°C, 1 to 24 hours, b) 1050°C, 1 to 15 hours, c) 600°C, 24 hours + 1050°C, 1 to 15 hours and d) 1050°C, 1 to 5 hours + 600°C, 1 to 10 hours.

Specimens for TEM analyses were prepared by a modified jet thinning procedure. Horizontal sections were prepared by

first immersing in a calibrated (9:1) HNO_3: HF etch solution to remove material within damaged regions and subsequently jet thinning from the front surface. Vertical cross section samples were prepared from a series of stacked 800 μm x 3000 μm strips cut along a <110> direction and embedded in epoxy resin (EPON-812). After chemical/mechanical polishing to a thickness of $\simeq$150 μm, specimens were ion milled in a Commonwealth Scientific instrument.

Secondary ion mass spectrometry was used to obtain oxygen impurity profiles at the back surfaces of the Si. Samples for cross-sectional SIMS imaging[25] were cleaved along a <110> direction, embedded in a low melting point Sn-Bi alloy, and subjected to chemical/mechanical polishing. In all cases, specimens were analyzed in a Cameca IMS-3f microanalyzer using Cs^+ ion bombardment while detecting $^{16}O^-$ and $^{30}Si^-$ secondary ions. The oxygen concentration levels were determined using standards prepared by ion implanting oxygen into CZ-Si. Residual pressure within the sample chamber during SIMS profiling was $\simeq 1 \times 10^{-9}$ Torr while sputtering at a rate of 350 Å/sec.

Transmission electron microscopic examination showed that the rotary abrasion process produced a laterally discontinuous array of nested dislocations decreasing in density as a function of depth beneath the level of macroscopic damage grooves. Annealing at 600°C for 1 to 24 hours in either vacuum or flowing N_2 produced no significant annihilation of dislocation line structure; however, dark field electron micrographs showed the presence of small (< 250 Å image diameter) microprecipitates within back surface damage regions either pinned along dislocation lines or in adjacent regions, increasing in density as a function of increasing

annealing duration. Examination of double annealed (600°, 24 hour + 1050°C, 1-3 hour) samples showed a dramatic increase in dislocation line concentration (Fig. 26a) and a subsequent increase in the effective width of the damage region at the back surface. In addition, we observed the appearance of well defined SiOx precipitates along dislocation lines and precipitate-dislocation complexes (PDC) associated with the nucleation of clustered precipitates (Fig. 26b)).

Figure 27 shows the measured dislocation line as a function of depth beneath damage grooves. In the damaged control samples and in samples annealed at 600°C for 24 hours, we observed a vertically graded dislocation line structure extending to an estimated depth of $\simeq 10\,\mu m$. After a double annealing, in either vacuum or flowing N_2, we observed a significant increase in the dislocation line density within the near surface ($< 10\,\mu m$) region and a zone of secondary line structure extending to a depth $\leq 40\,\mu m$.

To provide further information on the depth distribution of primary and secondary damage, we prepared vertical cross section samples for TEM analysis. Damaged (unannealed) and 600°C annealed samples contained dislocation lines extending to a depth $\simeq 10\,\mu m$, in agreement with horizontal sectioning measurements. Examination of double annealed (600°C + 1050°C) samples ([110] surface) showed a heavy concentration of dislocation lines and precipitates within a near surface region (depth $\leq 14\,\mu m$) and a secondary zone of dislocation lines extending from the periphery of the region to a depth of $40\,\mu m$. Figure 28 is a representative (vertical cross section) electron micrograph obtained at the edge region of the two zones ($d \simeq 14\,\mu m$) showing the development of secondary microstructure and precipitation within the primary damage region.

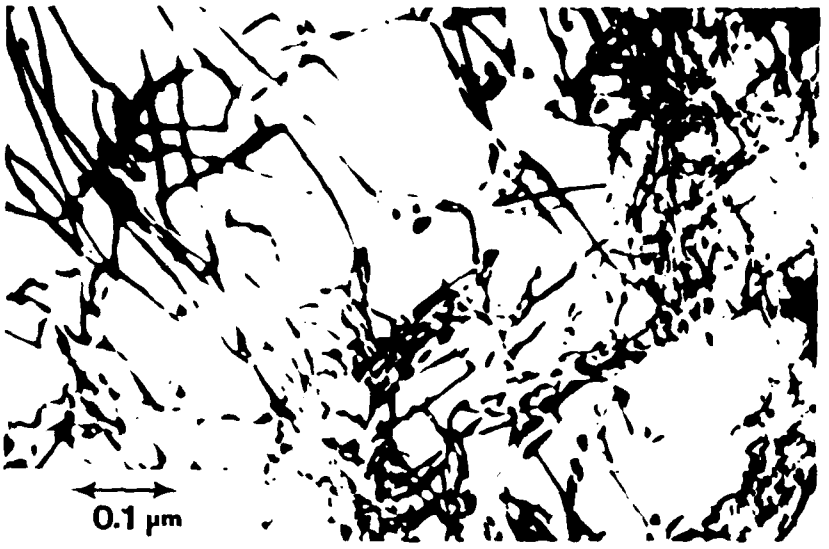

(a)

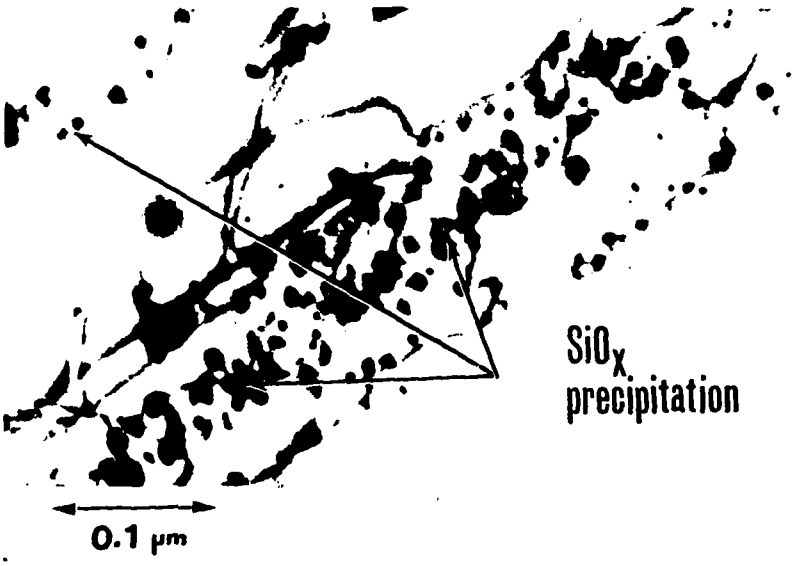

(b)

FIG. 26. BRIGHT-FIELD TRANSMISSION ELECTRON MICROGRAPHS OBTAINED ON BACK-SURFACE DAMAGED SAMPLES SUBJECTED TO VACUUM ANNEALINGS AT 600°C, 24 HRS. + 1050°C. 3 HR: (a) HORIZONTAL SECTION AT DEPTH OF ≈ 5 μm BELOW THE DEPTH OF DAMAGE GROOVES: (b) HIGH MAGNIFICATION MICROGRAPH SHOWING THE PRESENCE OF DISLOCATION LINES NUCLEATED WITHIN CLUSTERED SiOx REGIONS.

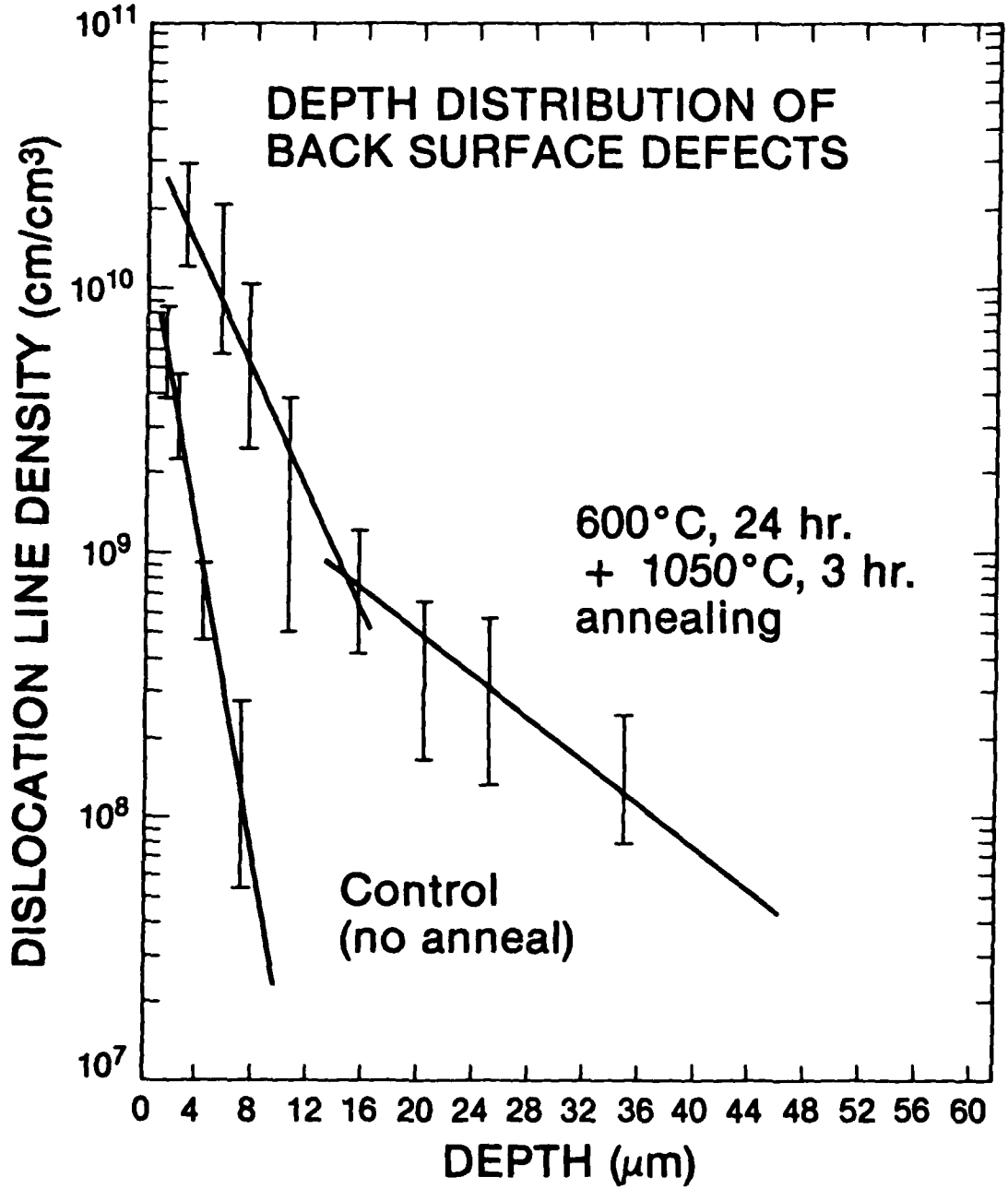

FIG. 27. DISLOCATION LINE DENSITY AS A FUNCTION OF DEPTH FOR CONTROL AND DOUBLE ANNEALED SAMPLES.

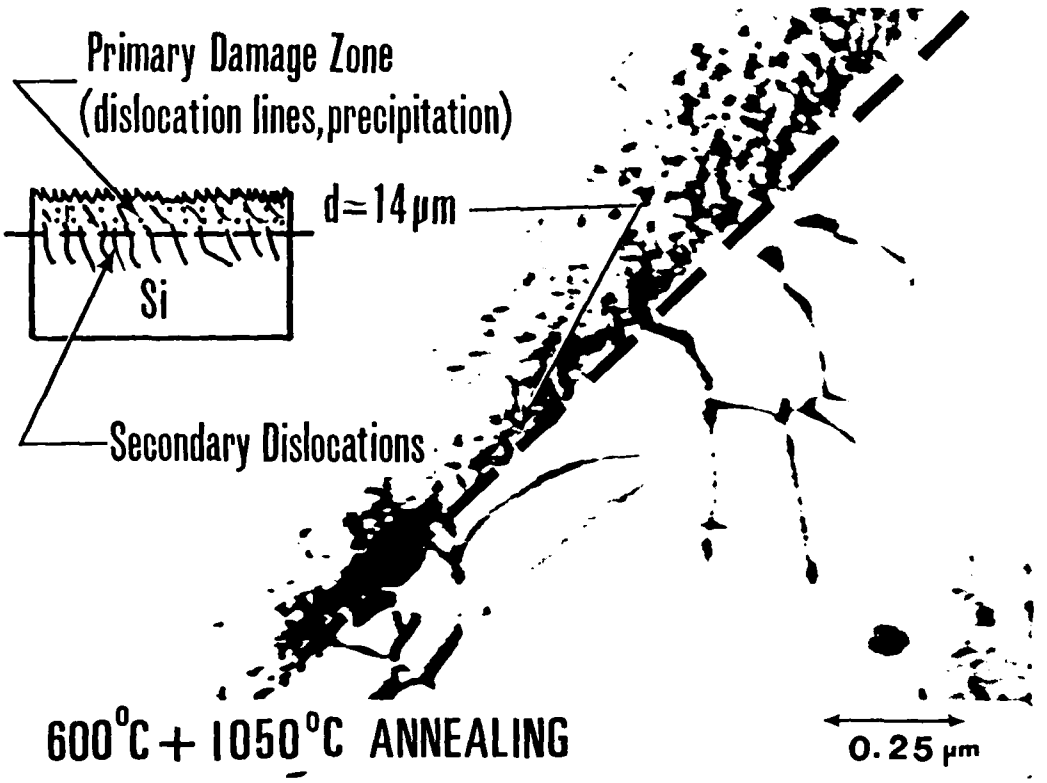

FIG. 28. BRIGHT-FIELD ELECTRON MICROGRAPHS OBTAINED ON VERTICAL CROSS-SECTION SAMPLES ([100] PLANE) AT DEPTH OF ≃ 14 μm AFTER ANNEALING AT 600°C FOR 24 HRS. FOLLOWED BY A 3-HRS. ANNEAL AT 1050°C.

Horizontal sectioning measurements show that $\simeq$ 80% of the dislocation line structure is annihilated after a 3-hour, 1050°C anneal. If this high temperature step is followed by 600°C annealing, the development of secondary dislocation line structure (Fig. 28) is not observed.

A correlation between dislocation line structure and oxygen redistribution was obtained from SIMS profiles of the oxygen concentration beneath damage grooves. Figure 29 shows the SIMS oxygen profiles in control (unannealed) and annealed samples. The control sample shows essentially no redistribution of oxygen, whereas annealing at 1050°C for 1 to 3 hrs. causes oxygen redistribution. Annealing at 600°C for 24 hours produces substantial motion and gettering of oxygen into back surface damage regions. Comparing Figs. 27 and 29 we observe that the oxygen is gettered within a region corresponding to the near surface dislocations. Correspondingly, when the low temperature annealing is followed by a 3 hr., 1050°C annealing treatment, the oxygen profiles again closely parallel the dislocation line density distribution shown in Fig. 27.

Ion micrographs (Fig.30) obtained on vertical cross-sections of annealed samples provide further supportive data on the correlation between oxygen redistribution and damage structure. After annealing at 600°C, dislocation lines are decorated with oxygen atoms and extend to a depth of $\simeq$ 10 μm. After subsequent annealing at 1050°C, the oxygen concentration is dramatically increased within the near surface region, producing a band of precipitated oxygen (Fig. 30b)). Secondary dislocation lines decorated with oxygen extend from the edge of the primary damage zone to a depth of $\simeq$ 40 μm. We detected <u>no</u> internal oxygen banding or secondary damage structure with correlated oxygen precipitation in undamaged or 1050°C annealed samples.

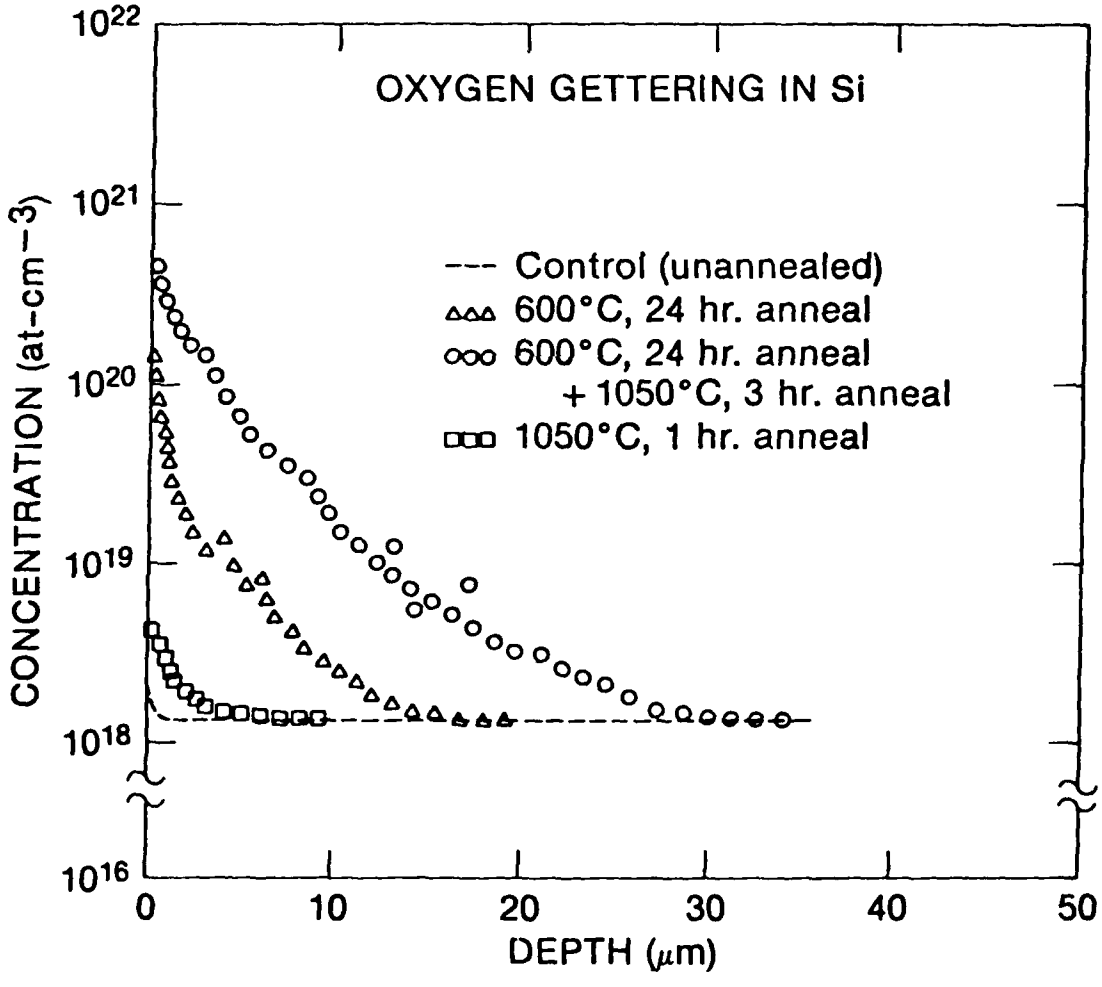

FIG. 29. SIMS PROFILES OF OXYGEN CONCENTRATION AT BACK SURFACE IN DAMAGED, ANNEALED SAMPLES.

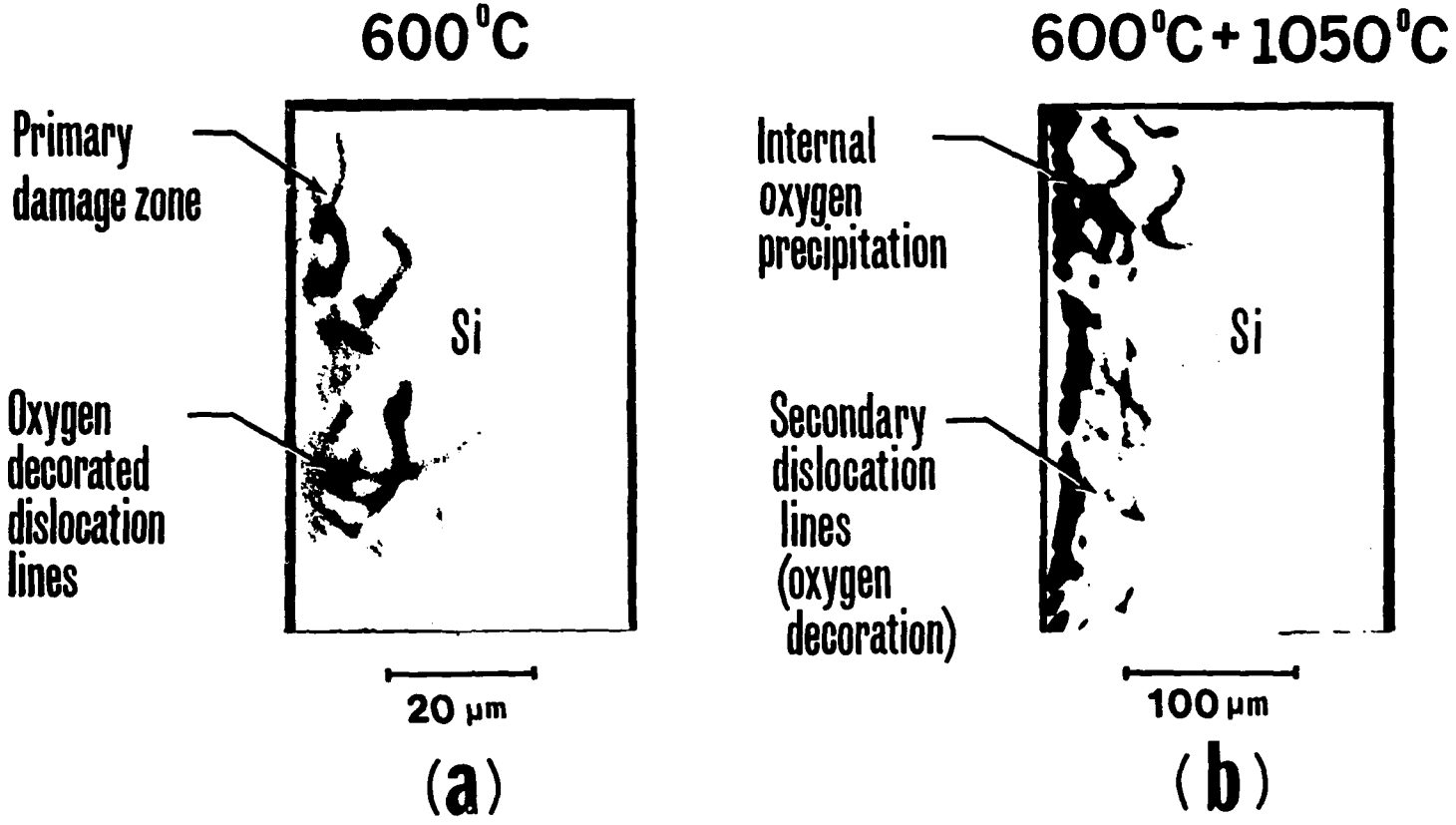

FIG. 30. SECONDARY-ION MICROGRAPHS SHOWING OXYGEN IMAGES OBTAINED ON [100] PLANES WITHIN BACK-SURFACE DAMAGE REGIONS OF WAFERS SUBJECTED TO ANNEALINGS: (a) 600°C, 24 HRS: (b) 600°C, 24 HR + 1050°C, 3 HR. NEGATIVE PRINTS ARE SHOWN FOR ENHANCED CONTRAST.

From this data we conclude that annealing of back surface damaged samples at 600°C produces rapid redistribution and gettering of mobile oxygen along dislocation lines. This primary damage is stablized or pinned in the presence of oxygen[26], with negligible annihilation upon further annealing at 600°C. Subsequent annealing at 1050°C produces additional gettering, oxygen precipitation and an increase in dislocation line density both within PDC clusters and as a result of increased strain fields created by the excessive SiO_x precipitation. Secondary dislocation lines extending to a depth of $\simeq 40\mu m$ are thought to be generated by large strain fields associated with misfit between SiO_x precipitates and the Si lattice within a heavily precipitated near-surface region. After forming, the secondary dislocation lines serve as sinks for additional gettering of oxygen. Hence, we can conclude that the observed results are related to a rapid diffusion and gettering of mobile oxygen from the bulk background oxygen concentration, with perhaps a small contribution from the surface.

8.2 LOW TEMPERATURE REDISTRIBUTION AND GETTERING OF OXYGEN IN SILICON

To extend the results of the initial investigation on the rapid redistribution of oxygen, a series of experiments were conducted using transmission electron microscopy (TEM), secondary ion mass spectrometry (SIMS) depth profiling and secondary ion microscopy to determine if oxygen can be gettered at temperatures in the range, 300° to 500°C.

Samples for these experiments were n- and p- type, 75 mm diameter, 400 μm thick CZ-Si wafers of [100] orientation. Oxygen and carbon concentrations of 1.0 to 1.1 x 10^{18} cm^{-3}

and 1.9 x $10^{16}cm^{-3}$, respectively, were determined by Fourier transform infrared (FTIR) absorption measurements on unannealed wafers using ASTM procedures[27]. Rotary abrasion techniques[28,29] were used to create concentric grooves of 8 to 10 μm depth into the back surfaces of wafers. Annealing was done in either flowing Ar or in an oil-free vacuum system at a pressure of $\simeq 10^{-8}$Torr. Samples were annealed in separate experiments at temperatures between 300° and 500°C for periods of 10 to 72 hours.

Control and annealed samples were prepared for TEM analysis in the form of 3mm x 3mm parallelopipeds. Conventional jet thinning techniques were used to produce electron transparent regions (<3500 Å thick) for examination in the electron microscope. Horizontal sectioning was used to obtain a quantitative measurement of the distribution of microstructural damage as a function of depth at the back surface of damaged wafers.

Oxygen concentrations at the back surfaces of control and damaged, annealed samples were determined using SIMS depth profiling. For cross-sectional analysis, samples were cleaved along a <110> direction, and cut into 1 mm x 5 mm strips. The strips were subsequently stacked and embedded in a low melting point Sn-Bi eutectic alloy. After chemical/mechanical polishing, the specimens were introduced into the chamber of the mass spectrometer and lateral oxygen distributions obtained in the ion imaging mode of operation[25]. All samples were analyzed in a Cameca IMS-3f microanalyzer using Cs^+ primary ion bombardment while detecting $^{16}O^-$ and $^{30}Si^-$ secondary ions. Calibration standards for determining oxygen concentrations were prepared by ion implantation of ^{16}O into CZ-Si.

Examination by TEM of control (undamaged) and back surface damaged (unannealed) samples showed that a laterally discontinous complex network of dislocation nests and tangles extending to a depth of >10 μm was produced by the rotary abrasion process. The dislocation density was observed to decrease as a function of depth, resulting in a vertically graded defect distribution at the back surface of the Si wafer. After annealing at temperatures in the range, 300° to 500°C, for periods of up to 72 hours, we observed no significant alterations in either the lateral or vertical distribution of defects within damaged regions. Careful examination of samples annealed at 300°C for 48 hours showed the presence of small microprecipitates (≈ 100 to 150Å average image diameter) concentrated at the edges of dislocation lines. Increasing either the annealing time or temperature produced a corresponding increase in the density of microprecipitates, accompanied by only a small increase in average image diameter. In Fig. 31a) we show a representative bright field electron micrograph obtained from the back surface of a sample after annealing at 400°C for 72 hrs. in flowing Ar. The presence of precipitates is clearly noted and observed throughout the damage region. Figure 31b) shows a schematic of the vertical cross section ([110] plane) and oxygen ion micrograph obtained from a sample annealed at 400°C for 72 hrs. in flowing Ar. The presence of oxygen along dislocation lines at the back surface is readily observed in the secondary ion micrograph. The majority of oxygen-decorated dislocation line structure is confined to a depth of ≤ 10 μm, beneath damage grooves at the back surface, in agreement with horizontal depth sectioning/TEM determinations of dislocation density profiles. In contrast, examination of damaged, unannealed samples in vertical cross section show no oxygen-decorated dislocation line structures by TEM and an apparent absence of any imageable oxygen (by SIMS) within damage regions at the back surface.

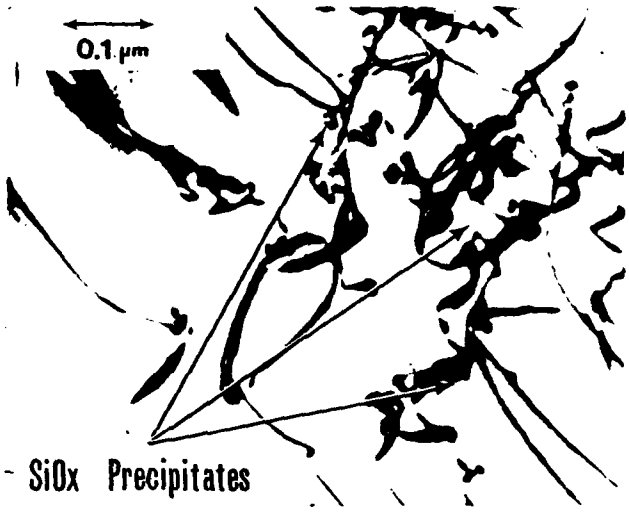

(a)

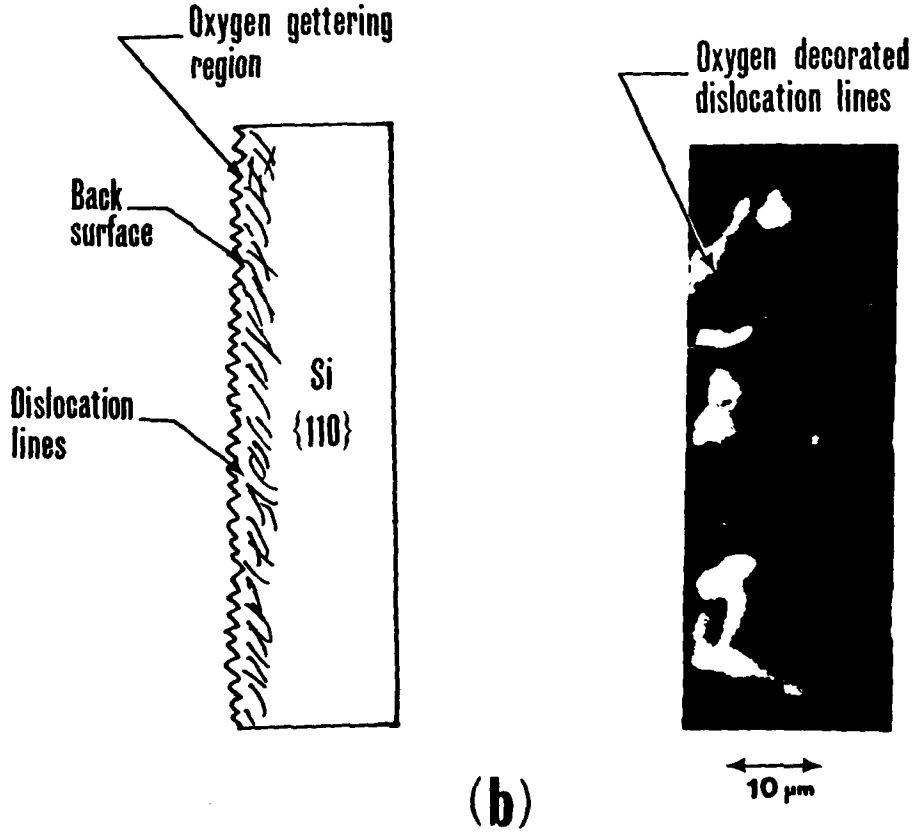

(b)

FIG. 31. BRIGHT-FIELD TRANSMISSION ELECTRON MICROGRAPH AND SECONDARY ION MICROGRAPH FROM BACK SURFACE DAMAGED Si SAMPLE AFTER ANNEALING AT 400°C FOR 72 HR; a) BRIGHT-FIELD ELECTROM MICROGRAPH SHOWING THE PRESENCE OF SiOx PRECIPITATES CONCENTRATED ALONG DISLOCATION LINES; b) SECONDARY ION MICROGRAPH AND SCHEMATIC SHOWING CROSS SECTIONAL SAMPLE ([100] PLANE) OXYGEN DECORATION ALONG DISLOCATION LINES WITHIN BACK SURFACE DAMAGE REGION.

To obtain additonal information on the redistribution of oxygen as a function of annealing temperature and annealing time, we obtained SIMS profiles of oxygen concentration as a function of depth beneath damage grooves at the back surface. Samples were annealed at 300°,350°,400° and 500°C for periods of 10 to 72 hrs. in separate experiments. For comparative purposes we conducted identical annealing experiments in flowing Ar and under high vacuum. Annealing at 300°C for periods <24 hrs. produced no detectable gettering of oxygen within damage regions. However, for annealing times >24 hrs. (at 300°C), we were able to clearly detect the presence of gettered oxygen at the back surface. Similarly, for annealing temperatures >300°C, the redistribution and gettering of mobile oxygen was noted within damage regions and observed to increase as a function of increasing annealing time. Figure 32 shows the relative $^{16}O^-$ion intensity profiles obtained at the back surface after damage introduction (no annealing) and after annealing at variable temperatures for 64 and 72 hrs. Also included for reference is the measured dislocation line density as a function of depth beneath damage grooves. After annealing at 300°C for 64 hrs., oxygen is concentrated within a zone < 2 μm wide at the back side of the wafer. When the temperature is increased to 350°C, the gettered oxygen is distributed over a region extending 8.0 μm below damage grooves at the back surface. After annealing at 400°C or 500°C for periods > 64 hrs. additional gettering of oxygen is noted throughout the damage region, resulting in a graded concentration profile that reflects the decreasing dislocation line density with increasing depth from the back surface. In comparative tests on vacuum annealed samples and samples annealed in flowing Ar, no essential difference in the distribution of gettered oxygen is observed in the profiles obtained, suggesting that the annealing process is not a significant oxygen source in these experiments.

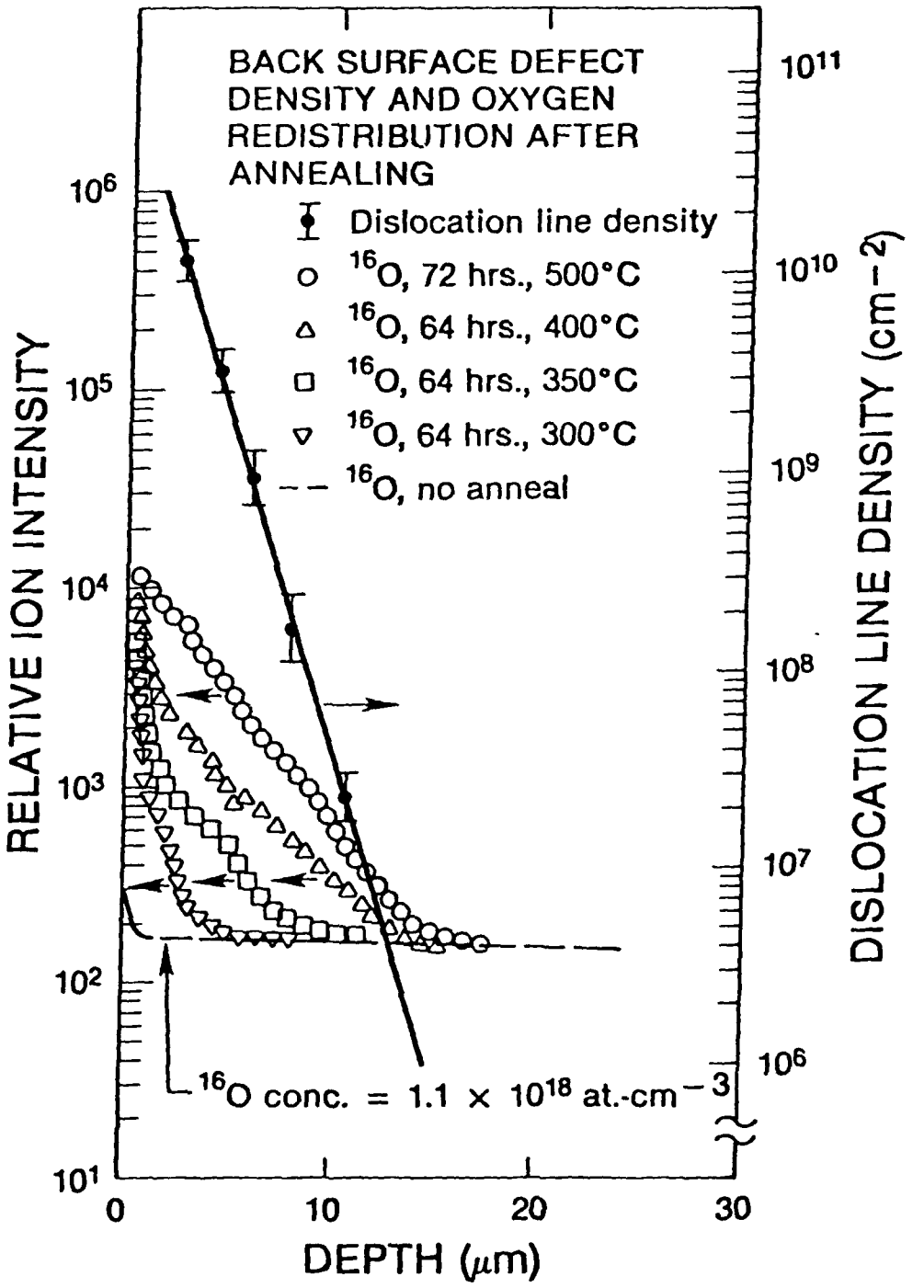

FIG. 32. BACK SURFACE DEFECT DENSITY AND SIMS PROFILES OF RELATIVE ^{16}O ION INTENSITIES AFTER ANNEALING AT VARIABLE TEMPERATURES.

Figure 33 shows a semilog plot of the gettered ^{16}O content as a function of $10^3/T(°K)$ for samples annealed for 48 and 72 hrs. at variable temperatures. The amount of gettered oxygen was obtained by integrating the oxygen concentration profiles over the gettering depth, relative to the back surface, with the limit of integration set at the point where the oxygen (gettered) profile intersects the background or bulk oxygen doping level ($1.1 \times 10^{18}/cm^3$). Using the data shown in Fig. 33 an activation energy of 0.92 ± 0.04 eV was computed.

The above data indicate that oxygen is rapidly redistributed and gettered by back surface damage at temperatures as low as 300°C. The process can be characterized by an activation energy of o.92 eV in the presence of a large stress field provided by the vertically graded dislocation line density at the wafer backside. Both transmission electron and secondary ion micrographs confirm the presence of oxygen-related (SiOx) precipitates along dislocation lines. Correlated SIMS profiles also show a graded oxygen profile indicative of the decreasing dislocation line density as a function of depth. From this data we can negate the possibility of enhanced motion of the oxygen via a dislocation line/pipe diffusion mechanism, since transport along a diffusion pipe would not result in a graded oxygen profile. Furthermore, the flux of oxygen atoms moving from the interior of the wafer to the backside would require an additonal driving force fo accelerated mass transport.[30] Hence, it appears that the low temperature diffusion and gettering of oxygen observed in these experiments is largely controlled by the magnitude of the stress gradient at the back surface. It can be speculated that similar low temperature diffusion of oxygen will occur in the presence of a stress field, whether such fields are introduced by ion implantation damage, precipitation or contact alloying.

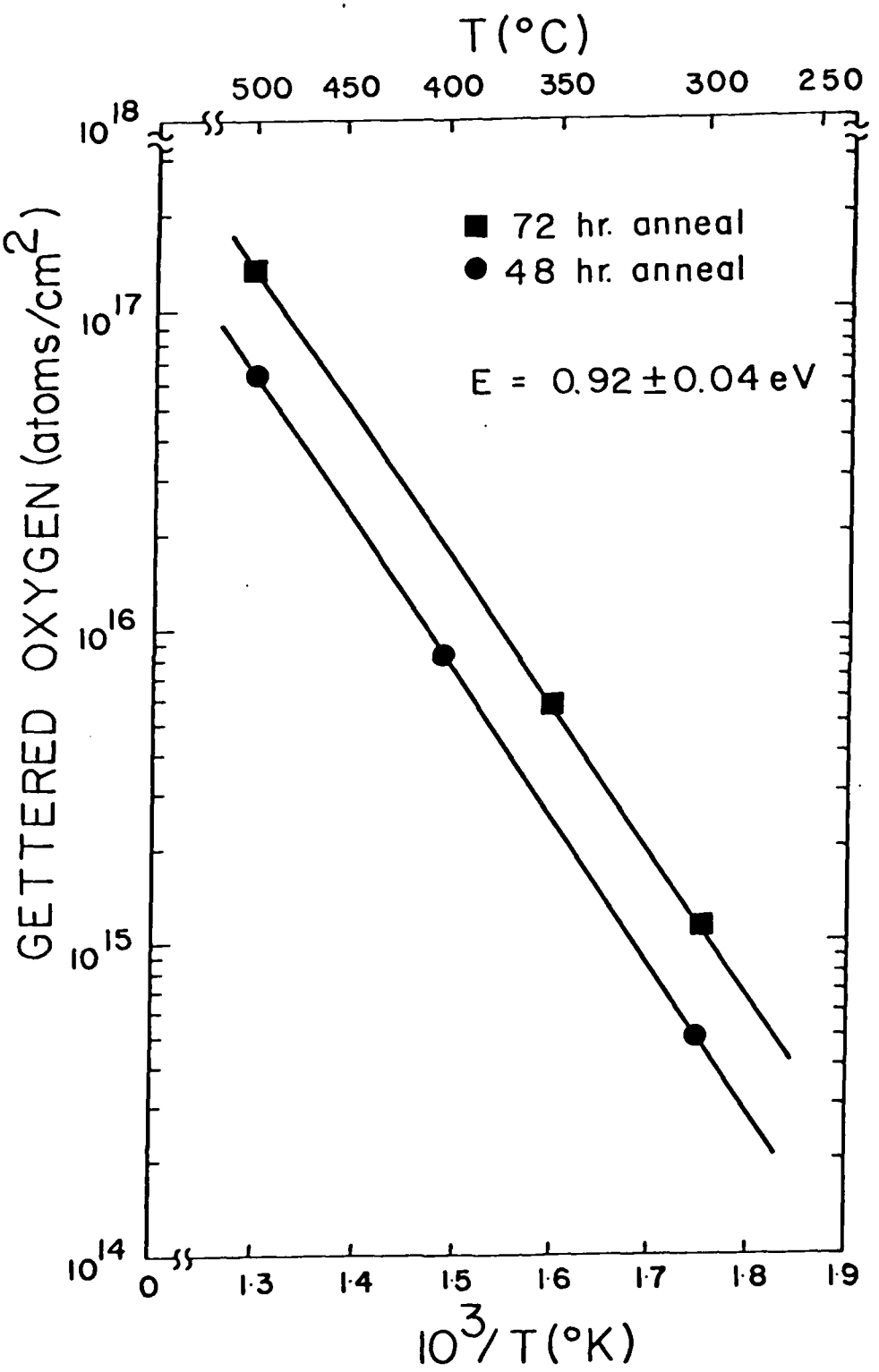

FIG. 33. BACK SURFACE GETTERED ^{16}O CONCENTRATION VS. RECIPROCAL TEMPERATURE FOR 48- AND 72-HR. ANNEALING PERIODS.

8.3 REDISTRIBUTION OF OXYGEN WITHIN DAMAGE REGIONS OF BORON IMPLANTED SILICON

The role of oxygen in influencing the electrical properties of silicon has received considerable attention over the past ten years. With the increasing demand for more detailed information on impurity redistribution and process-induced alterations in material properties, the subject of oxygen redistribution in Si has remained an illusive topic, and inferences have typically been drawn from bulk infrared absorption measurements on Si wafers. However, such techniques have limited utility in the investigation of localized redistribution of oxygen within regions of importance to device technology.

Using secondary ion mass spectrometry (SIMS) profiling, secondary ion microscopy and transmission electron microscopy, it has been recently demonstrated[31,32] that oxygen is rapidly redistributed and gettered within damage regions created by mechanical abrasion at the wafer backside. The data indicated that oxygen was extremely mobile at temperatures between 300°C and 1050°C, and that strain fields created by the presence of damage in the Si lattice was an important factor in the enhanced diffusion of oxygen in Si.

In an earlier paper Koyama[33] investigated the redistribution of ^{18}O in Si wafers implanted with ^{18}O and subsequently annealed at 900°C to 1100°C. He observed a complicated redistribution of ^{18}O after annealing and noted prominent gettering of ^{18}O within its own implant damage zone. However, instrumental limitations on the detection capabilities of common ^{16}O ($\leq 4 \times 10^{19}$ atoms/cm^3) precluded any detailed resolution of the induced redistribution of the natural oxygen incorporated during Si crystal growth. In the present and

previous studies, we have shown that the contribution of extraneous sources in the current SIMS instrument (Cameca IMS-3f) can be reduced to provide an ^{16}O detection limit of $<3 \times 10^{17}$ atoms/cm^3.

In this study we were concerned with the investigation of bulk oxygen redistribution in B-implanted Si after typical annealing at 900°C to 1000°C and the influence of secondary annealing treatments on oxygen redistribution after primary post-implant thermal annealing. This paper presents data from TEM and SIMS analyses and discusses the implications of data obtained.

Silicon wafers (p-type) used in this study were grown by the Czochralski (CZ) technique and were of [100] orientation. Samples were of 75 mm diameter and $\sim$ 400 m thick. A background oxygen concentration of 1.2×10^{18} atoms/cm^3 was determined on unannealed control wafers by Fourier transform infrared (FTIR) absorption measurements using ASTM procedures[27].

Wafers were implanted at room temperature with 50 keV B-ions to a total dose of 10^{15}/cm^2. In separate experiments primary annealing (post-implant) was done in a flowing Ar atmosphere at temperatures of 900°C and 1000°C for a period of 1 hour. Secondary annealing was performed under similar conditions at temperatures of 500°C and 600°C for periods of 1 to 3 hours.

Samples for microstructural analysis were prepared in the form of 3 mm x 3 mm squares and subsequently jet thinnned to produce thin electron transparent regions for examination in the electron microscope. Specimens for SIMS analysis were

cut into 5 mm x 5 mm squares and oxygen depth profiling performed within the sample chamber of a Cameca IMS-3f ion microanalyzer, using Cs^+ ion bombardment while detecting $^{16}O^-$ and $^{11}B^-$ secondary ions. Oxygen concentration levels were determined using standards prepared by implanting ^{16}O ions into CZ-Si and FZ-Si.

Transmission electron microscopic examination of control (not implanted) samples showed an apparent absence of clearly resolvable microstructural defects within near surface regions of the wafer. After B-implantation and annealing at 900°C for 1 hr. (Fig. 34a)) we observe the nucleation of rod shaped structures, dislocation dipoles and dislocation loops, essentially in agreement with earlier results [34,35] reported by investigators. After annealing at 1000°C for 1 hr. we observe an annihilation and decomposition of rod shaped structures, leaving residual damage in the form of large dislocation loops, dislocation lines, dislocation ring structures and dipole remnants (Fig. 34b)). Under either anneal condition, we were unable to detect any significant concentrations of small microprecipitates that might be associated with SiOx nucleation.

After secondary annealing at 600°C for 1 to 3 hours, subsequent to the 900°C or 1000°C implant damage anneals we detected the presence of small microprecipitates ($\simeq$ 70 Å average image diameter) within the implanted region at depths 0.16 μm. These secondary microprecipitates were clearly detectable after secondary annealing of the 1000°C annealed samples. In Fig. 34c we show a representative bright field electron micrograph obtained from an implanted sample subjected to a 1000°C, 1 hr + 600°C, 3 hr. annealing treatment. It can be observed that secondary microprecipitates are clearly present within damage regions and along residual dislocation line structure. Extended anneals at 600°C produced

no apparent annihilation of the microprecipitates and no significant changes in concentration within the zone at R_p ($\simeq$ 0.16 μm). Examination of depth regions exceeding R_p showed an absence of secondary microprecipitation.

To determine the correlation between implant damage nucleation, secondary microprecipitation and oxygen redistribution we obtained SIMS profiles of ^{16}O concentrations after implantation and subsequent primary and secondary anneals at 900°C to 1000°C and 600°C, respectively. In Fig. 35 we show representative SIMS ion intensity profiles of the B and O distributions after implantation and annealing. The background oxygen concentration was determined to be $\simeq$ 1.2 x 10^{18} atoms/cm^3. The annealed sample shows only a narrow near surface zone of oxygen accumulation. After annealing at 900°C or 1000°C, we observe an increase in the surface concentration of ^{16}O, associated with apparent outdiffusion. However, within the implanted layer, we detect no evidence of gettered oxygen and the oxygen concentration is essentially identical to the level observed in the unannealed sample at depths corresponding to the region of maximum implantation damage.

In contrast, after secondary annealing at 600°C, following primary 900° or 1000°C annealing treatments, we observe prominently defined regions of oxygen gettering within damage zones. In samples annealed at 900°C (1 hr.) + 600°C (3 hrs.), the data show that oxygen is gettered near Rp, producing a well defined peak in the oxygen concentration profile. In addition, a wider zone of gettering can be noted, extending from the surface to a depth of $\simeq$ 0.12 μm. In separate experiments, if the primary anneal temperature is increased to 1000°C the low temperature 600°C anneal produces oxygen gettering at Rp, an apparent reduction in the near surface concentration of gettered oxygen observed in

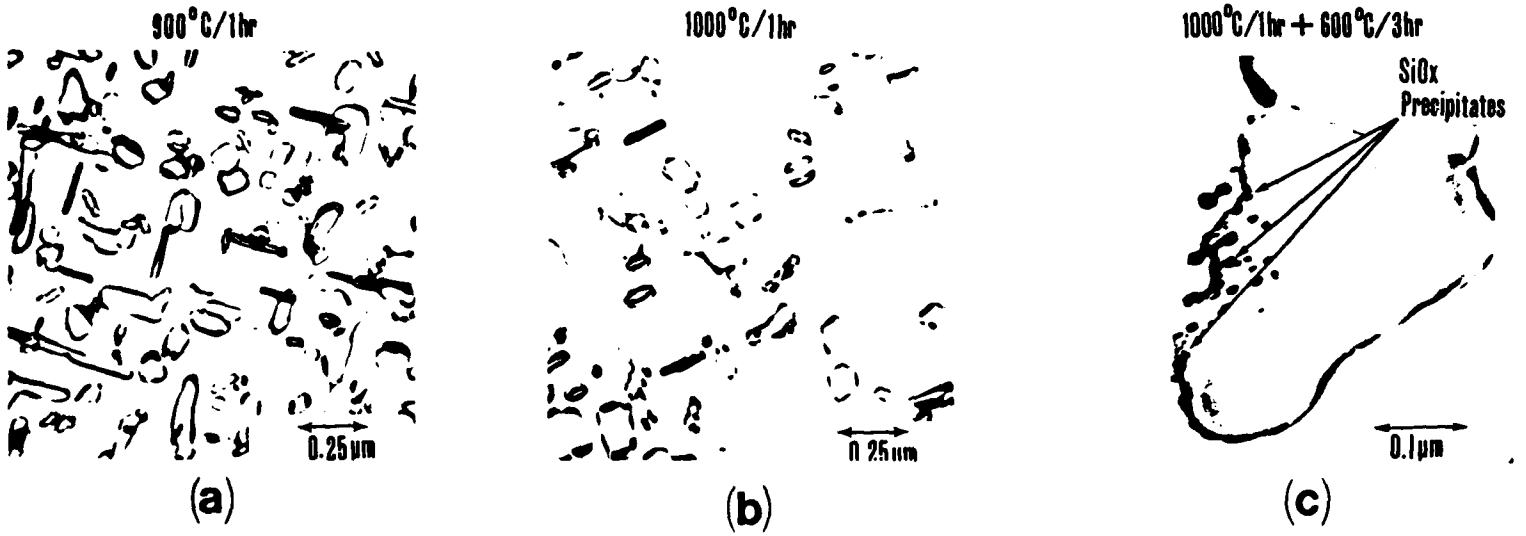

FIG. 34. REPRESENTATIVE BRIGHT-FIELD TRANSMISSION ELECTRON MICROGRAPHS OBTAINED FROM B-IMPLANTED SAMPLES AFTER ANNEALING; a) 900°C, 1 HR.; b) 1000°C, 1HR; c) 900°C, 1 HR + 600°C, 3 HR.

the 900°C + 600°C annealed samples, and outdiffusion of oxygen at the surface. In both cases, localized depletion of oxygen below the background doping level occurs at the edge of the gettered oxygen profile at depths > 0.22 μm.

Comparing the data shown in Figs.34 and 35 we can establish a correlation between the development of microstructural damage and gettering of oxygen. During the 900°C or 1000°C oxygen diffuses rapidly to the surface with only negligible trapping within the implanted region. However, once nucleated, residual defects serve as gettering sites for diffusing oxygen upon subsequent annealing.

The amount of gettered oxygen within the implanted region will depend upon the concentration and spatial distribution of residual damage retained after the primary annealing as shown in Figs. 34 and 35. Quantitative measurements of the peak ^{16}O concentration relative to background doping levels show a >35% increase in gettered oxygen content within the implanted region after secondary annealing. It is unknown at present whether multiple post-implant annealings at variable temperatures and times (as typically encountered in device processing) will substantially increase the amount of SiOx precipitation beyond that observed within the implanted region or whether secondary defects will result from the increased SiOx nucleation. In additon, it can be speculated that the (stable) SiOx precipitation will serve as trapping sites for fast diffusing metallic impurities introduced during device processing. In either case, additional studies are required to assess the implications of the rapid motion and gettering of oxygen into implantation damage zones.

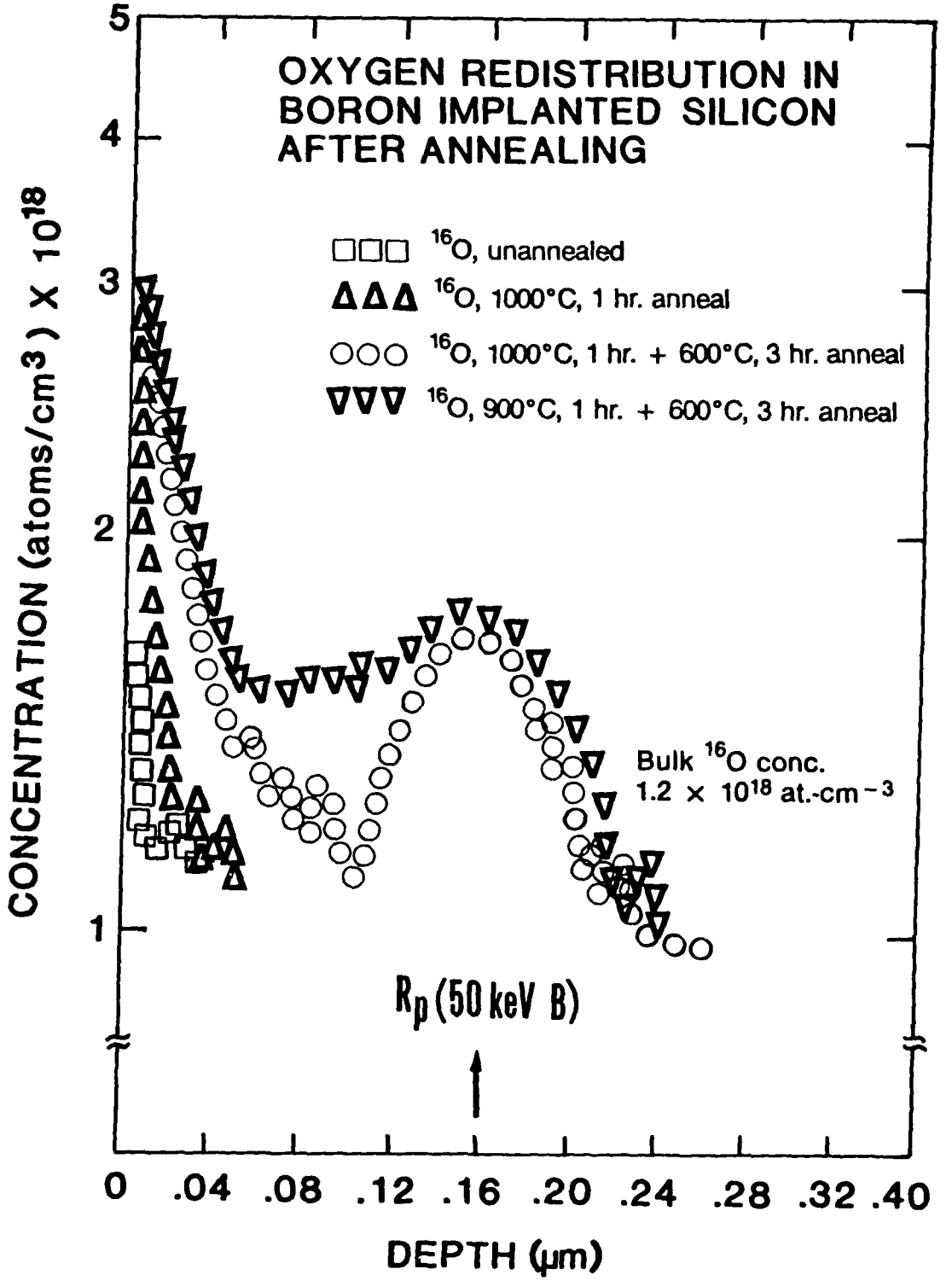

FIG. 35. SIMS DEPTH PROFILES OF ^{16}O AND ^{11}B CONCENTRATIONS AFTER B-IMPLANTATION AND ANNEALING.

8.4 THERMAL REDISTRIBUTION OF OXYGEN DURING SOLID PHASE REGROWTH OF ARSENIC IMPLANTED AMORPHIZED SILICON

Oxygen redistribution into localized damage regions in Si wafers has been reported[31-33,36,37] in a number of recent reports. At the present time, however, there have been no detailed investigations of the localized gettering of oxygen into amorphizing ion implants in Si and of the redistribution of oxygen during solid phase regrowth of the implanted layer. Of equal importance is the current lack of correlation between residual defect structure retained after single crystal regrowth of the amorphous layer and the nature of oxygen redistribution within reordered zones. In this paper, we present the results of an investigation of oxygen redistribution in As-implanted (111) Si, utilizing correlated data obtained from scanning electron microscopy (SEM), transmission electron microscopy/diffraction (TEM/TED), secondary ion mass spectrometry (SIMS) and secondary ion microscopy.

Silicon samples (p-type) used in this study were of (111) orientation ($\pm$ 1°) and grown by the Czochralski (CZ) technique. The wafers were of nominal 75 mm diameter and $\simeq$400 μm thick. Preliminary determinations of oxygen concentration in as-received wafers were made using Fourier transform infrared (FTIR) absorption and ASTM standards[27]. Measured oxygen concentrations were found to lie within the range, 1.5 to 1.8 x 10^{18} at-cm^{-3}.

After conventional surface cleaning, specimens were clipped onto the stage of a rotary carousel unit within the sample chamber of the ion implantation machine. Samples were then implanted at room temperature with 200 keV As-ions to a dose of 10^{15}/cm^2. Following implantation, the

wafers were annealed in a flowing Ar atmosphere at temperatures in the range, 400 to 1000°C, for 1/2 to 4 hr.

Control (unannealed) and annealed samples were prepared for TEM/TED analysis in the form of 3mm x 3mm squares. Conventional chemical jet thinning and stripping techniques were used to produce thin regions for examination in the electron microscope. Samples were cut into 5mm x 5mm squares for SIMS profiling and secondary ion microscopy measurements. Impurity depth profiling was obtained using a Cameca IMS-3f ion microanalyzer and Cs^+ ion bombardment while detecting $^{16}O^-$ and $^{75}As^-$ secondary ions. Oxygen and arsenic concentration levels were determined using standards prepared by implanting ^{16}O and ^{75}As ions into CZ and FZ-Si.

Transmission electron microscopic examination of implanted, unannealed samples showed the presence of an amorphized layer, with no evidence of crystallinity within the implanted zone. After annealing at 800°C for 1 hr., crystallinity was restored, leaving a highly disordered residual damage region (Fig. 36a). Extended defects in the form of twins, stacking faults and dislocation lines are noted throughout the implanted region, extending to the surface of the samples. These results are similar to earlier reported data on regrowth of amorphous layers produced by implantation of Si ions into (111) Si wafers [38]. After annealing at 900°C or 1000°C (Figs. 36b and 36c)), we observe that the density of extended defects remains high even when the annealing temperature is increased. Of importance, however, is the observation of small precipitates noted along dislocation lines and stacking faults. These defects are not readily removed by heat treatments and persist throughout the annealing sequence. Since point defect clusters associated with radiation damage are largely annealed at the higher temperatures, the presence of defects selectively pinned along

dislocation lines and stacking fault zones cannot be related concentrations do not permit the composition of these precipitate regions to be readily identified by conventional selected area diffraction techniques.

To determine more about the localized distribution of impurities and the possibility of SiOx nucleation within the implanted region, SIMS chemical profiling was obtained on implanted, annealed samples. Figure 37 shows representative ^{16}O and ^{75}As concentration profiles obtained from control (implanted, no anneal) and annealed samples subjected to various annealing temperatures. After implantation, we observe no distinct or identifiable redistribution of oxygen within control samples. However, after annealing for 1 hr. at 800°C or 1000°C we observe four distinct zones of oxygen redistribution within the implanted samples. The near surface zone, extending to a depth of $\simeq$ 500Å, is characterized by a large pileup of oxygen, increasing in concentration as a function of annealing temperature. The next zone of oxygen redistribution is observed at depths approximately equal to the projected range, R_p, of the implanted ion ($\simeq$1100Å), where sharply defined regions of oxygen gettering are detected. At depths $R_p + \Delta R_p$ (1500 Å) a secondary oxygen gettering region is noted in all samples examined. At depths exceeding $R_p + \Delta R_p$, detectable oxygen depletion occurs over a region extending to a maximum depth of $\simeq$ 1 μm.

In samples annealed (in separate experiments) at temperatures between 600 and 1000°C, we also observe an increasing oxygen concentration within damage zones at R_p and $R_p + \Delta R_p$ as the annealing temperature is increased. In addition, the amount of oxygen pileup and outdiffusion at the surface is altered significantly as the annealing temperature is varied between 600° and 1000 °C. Correspondingly, the width of

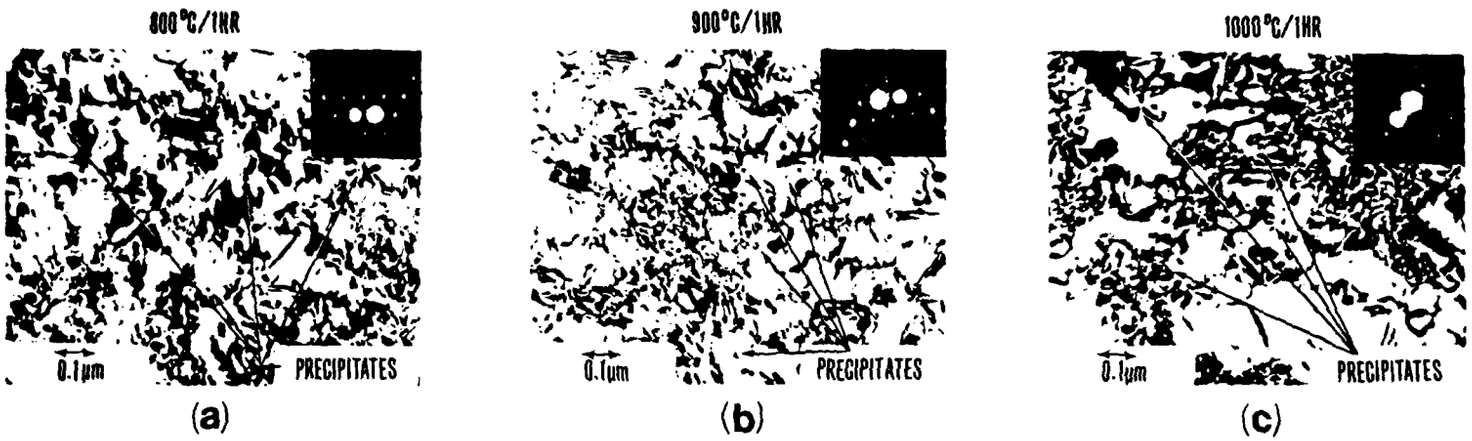

FIG. 36. REPRESENTATIVE BRIGHT-FIELD ELECTRON MICROGRAPHS OBTAINED FROM IMPLANTED SAMPLES AFTER 1 HR. ANNEALS: a) 800°C; b) 900°C; c) 1000°C.

the oxygen depletion region is enlarged as the annealing temperature is elevated and the amount of gettered oxygen in implanted regions is increased.

To further investigate the influence of residual damage nucleated during solid phase regrowth on the gettering of oxygen, we conducted a series of experiments in which low temperature (400° to 600°C) heat treatments were performed after primary annealing at 900°C or 1000°C. We observed additional gettering of oxygen within zones at R_p and $R_p + \Delta R_p$, in direct proportion to annealing temperature and anneal duration. In all cases, we observed no reduction in the gettered oxygen concentration (reverse annealing) after secondary annealing, suggesting that damage nucleated during solid phase regrowth will also be effective in additional gettering of mobile oxygen during subsequent thermal processing. This is consistent with TEM data that shows stability of residual extended defect structure over a wide range of annealing conditions.

Since secondary low temperature anneals produce measurable increases in gettered oxygen content and SiOx nucleation within damage zones, it would be interesting to determine the effect of a low temperature anneal preceding the high temperature annealing treatment. To address this issue, we annealed implanted samples at 400°C for 1 to 4 hrs., followed by annealing at 900 or 1000°C in separate experiments. In Fig. 38, we show representative SIMS profiles of the oxygen redistribution in a single and doubled annealed samples. After 400°C annealing, we observe no detectable redistribution of oxygen within the implanted region. After two stage annealing (400°C + 1000°C), we observe a single oxygen gettering peak at R_p with the anticipated surface accumulation and depletion of oxygen at depths exceeding R_p. Comparing Figs. 37 and 38 , we note the apparent absence of a second gettering peak at $R_p + \Delta R_p$. These experiments

AD-A104 180 ADVANCED RESEARCH AND APPLICATIONS CORP SUNNYVALE CA F/G 20/12
INVESTIGATION OF IMPURITY REDISTRIBUTION EFFECTS AND SOLUBILITY--ETC(U)
JUN 81 T J MAGEE, C LEUNG, R ORMOND N00014-80-C-0482

UNCLASSIFIED NL

2 OF 2
AD A
104180

END
DATE FILMED
10-81
DTIC

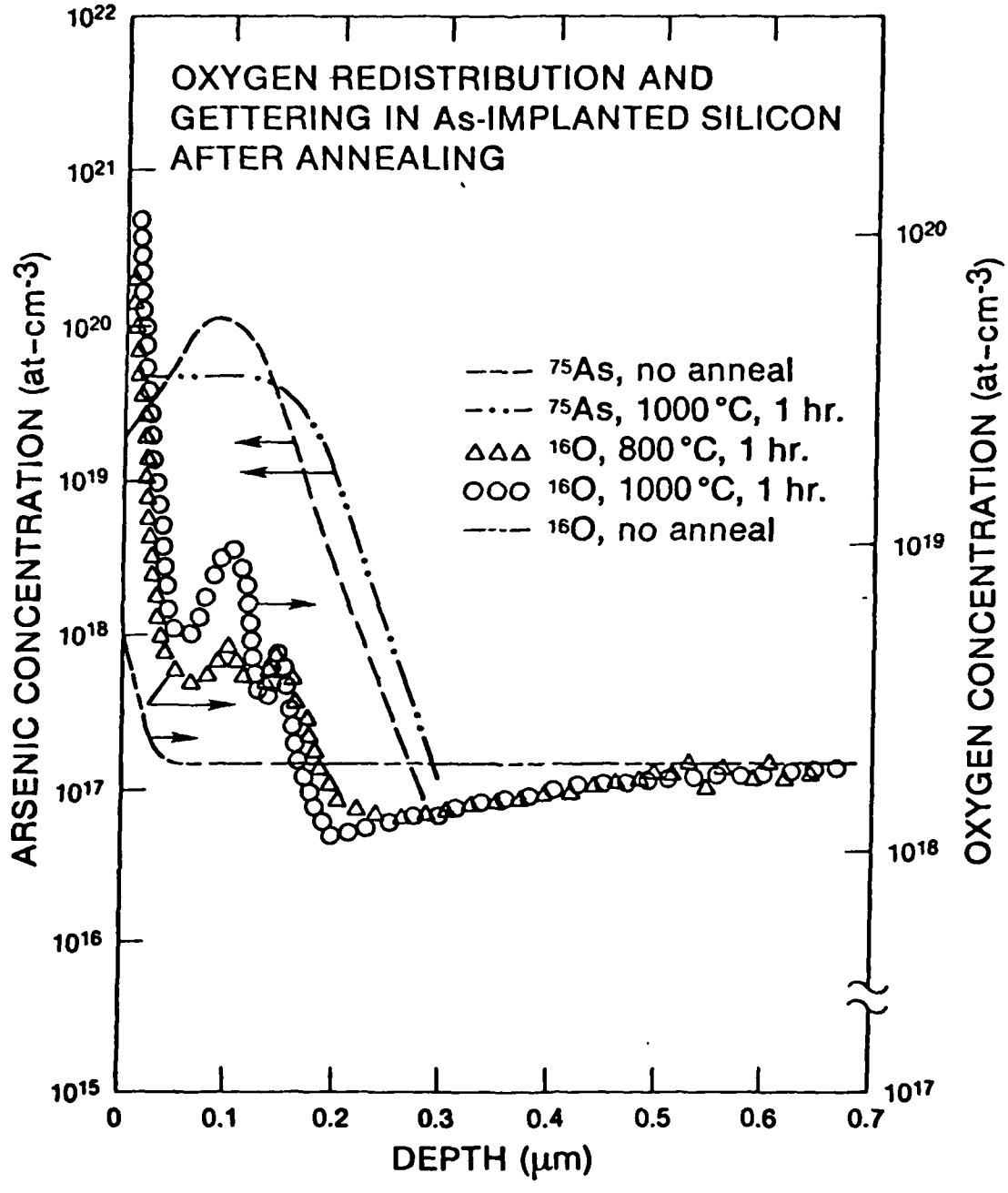

FIG. 37. SIMS PROFILES OF ^{75}As AND ^{16}O CONCENTRATIONS IN IMPLANTED AND ANNEALED SAMPLES.

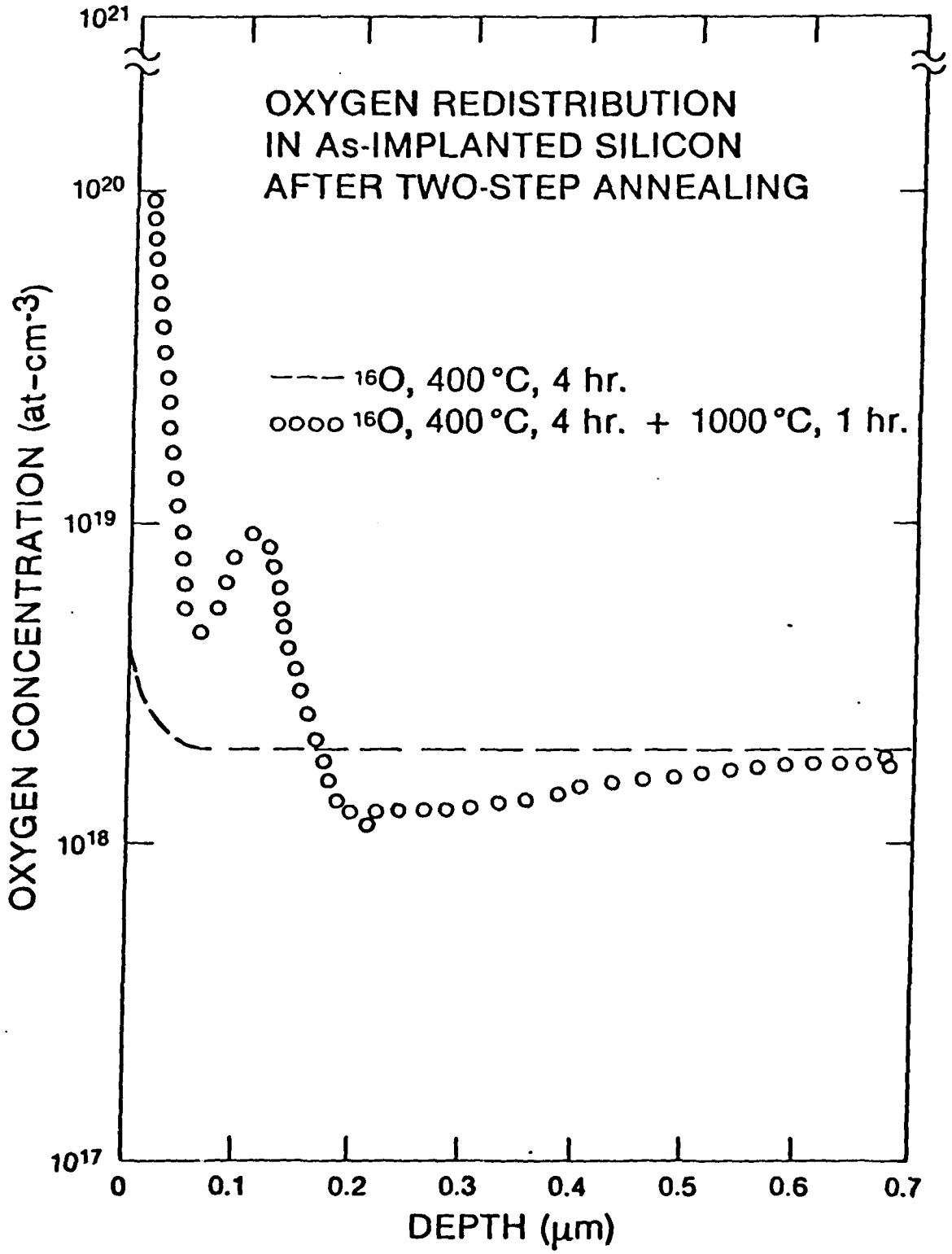

FIG. 38. SIMS PROFILES OF ^{16}O CONCENTRATIONS AFTER SINGLE AND DOUBLE ANNEALS.

were then repeated using the same annealing conditions and the results obtained were essentially identical. At 900°C we also observe a qualitatively similar pattern of oxygen redistribution, with an absence of the secondary oxygen gettering peak.

Subsequent TEM examination of implanted, unannealed samples showed the presence of small ($\leq$150Å) clustered defects within a narrow region at depths $\simeq$ 1500 Å from the surface. After annealing at 400°C for 1-4 hrs., the clustered regions are largely annihilated. The remainder of the implanted region retains the amorphous character of the zone, with no subsequent defect nucleation or reordering by solid phase regrowth. Since the region at 1500Å represents a transitional zone between the amorphized and single crystal regions, low temperature annihilation of point defect clusters will effect both solid phase regrowth and residual defect nucleation in the interfacial (transitional) region between these two areas. These results are in essential agreement with earlier investigations of low temperature effects on defect annihilation[39] and regrowth at the boundary region[38]. In the present study, we have shown for (111) Si that the effect of altering the initial defect concentration and character of regrowth defects by low temperature primary annealing is to eliminate oxygen gettering at the interfacial region ($d \geq R_p + \Delta R_p$) and reduce the total amount of gettered oxygen within the implanted region.

From the results obtained in this study we can conclude that oxygen is rapidly gettered into damage regions of As-implanted (111) Si during and subsequent to solid phase regrowth of the amorphized region. Additional thermal processing produces further increases in the amount of oxygen gettering and SiOx nucleation within the implanted region.

In all cases, pronounced surface pileup and outdiffusion of oxygen can be correlated with the presence of twins, stacking faults and residual defects extending throughout the implanted region to the surface of the sample. When low temperature anneal treatments precede conventional high temperature annealings, annihilation of defects at the amorphous/crystalline interface and subsequent reductions in residual regrowth defects at the interface during high temperature solid phase regrowth will result in reductions in the concentration of gettered oxygen at the interfacial region.

REFERENCES

1. A. M. Huber, G. Morilot, N.T. Linh, P.N. Favennec, B. Deveand and B. Toulouse, Appl. Phys. Lett. 34, 859(1979).

2. C. A. Evans, Jr., V. R. Deline, T. W. Sigmon and A. Lidow, Appl. Phys. Lett. 35, 291(1979).

3. P. N. Favennec and H. L. Haridon, Appl. Phys. Lett. 35, 699(1979).

4. T. J. Magee, J. Peng, J. Hong, C.A. Evans, Jr., V.R. Deline and R. M. Malbon, Appl. Phys. Lett. 35, 277(1979).

5. T.J. Magee, J. Peng, J.D.Hong, V.R. Deline and C.A. Evans,Jr.,Appl. Phys. Lett. 35, 615(1979)6. J. Kasahara

6 J. Kasahara and N. Watanabe, Japanese J. Appl. Phys. 19, L151(1980).

7. P.M. Asbeck, J. Tandon, B.M. Welch, C.A. Evans, Jr., and V.R. Deline, IEEE Electron Device Lett. EDL-1, 35(1980).

8. T. J. Magee, J. Hung, V.R. Deline and C.A. Evans, Jr., Appl. Phys. Lett. 37, 53(1980).

9. T.J. Magee, K.S. Lee, R. Ormond, R.J. Blattner and C.A. Evans, Jr., Appl. Phys. Lett. 37, 447(1980).

10. T.J. Magee, K.S. Lee, R.D. Ormond, C.A. Evans, Jr., R.J. Blattner and C. Hopkins, Appl. Phys. Lett. 37, 635(1980).

11. J. R. Arthur, J. Phys. Chem. Solids 28, 2261(1967).

12. L. J. van der Pauw, Philips Res. Rpts. 13, 1(1958).

13. C. G. Hopkins, V.R. Deline, R.J. Blattner, C.A. Evans,Jr., and T.J. Magee, Appl. Phys. Lett. 36, 989(1980).

14. P. K. Vasudev, R.G. Wilson and C.A.Evans, Jr., Appl. Phys. Lett. 37 308(1980).

15. B. M. Welch, North American Rockwell (private communication), (1980).

16. T. Y. Tan, E. E. Gardner and W. K. Tice, Appl. Phys. Lett. 30, 175(1977).

17. S. Kishino, S. Isomae, M. Tamura and M. Maki, Appl. Phys. Lett. 32, 1(1978).

18. K. Yamamoto, S. Kishino, Y. Mashushita and T. Iizuka, Appl. Phys. Lett. 36, 195(1980).

19. S. Kishino, M. Kanamori,, N. Yoshihiro, M. Tajima and T. Iizuka, Appl. Phys. 50, 8280(1979).

20. F. Shimura, H. Tsuya and T. Kawamura, Appl. Phys. Lett. 37, 483(1980).

21. Annual Book of ASTM Standards (ASTM, Philadelphia, 1977), Pt. 43, F-121.

22. T. J. Magee, J. Peng, J. D. Hong, C. A. Evans, Jr., V. L. Deline and R. M. Malbon, Appl. Phys. Lett. 35, 277(1979).

23. T. J. Magee, J. Peng. J. D. Hong. W. Katz and C. A. Evans, Jr. Phys. Stat. Sol. (A) 55, 161(1979).

24. J. E. Lawrence, Met. Soc. AIME 242 484(1968).

25. G. H. Morrison and G. Slodzian, Anal. Chem. 47, 932A (1975).

26. S. M. Hu, Appl. Phys. Lett. 31, 53(1977).

27. Annual Book of ASTM Standards (ASTM, Philadelphia, 1977), Pt. 43, F-121.

28. J.E. Lawrence, Met. Soc. AIME 242, 484 (1968).

29. T. J. Magee, J. Peng, J. D. Hong, W. Katz and C. A. Evans, Jr., Phys. Stat. Sol. (A) 55, 161 (1979).

30. P.G. Shweman, Diffusion in Solids, (McGraw-Hill, New York, 1971), Chap. 1.

31. T.J. Magee, C.Leung, H. Kawayoshi, B.K. Furman and C.A. Evans,Jr., Appl. Phys. Lett. (1981)(in press).

32. T.J. Magee, C. Leung, H. Kawayoshi, B.K. Furman, C.G. Hopkins and C.A. Evans,Jr., J. Appl. Phys. (1981) (in press).

33. H. Koyama, J. Appl. Phys.51,3202(1980).

34. R.W. Bicknell and R.M. Allen, Radiation Eff. 6,45(1970).

35. L.T. Chadderton and F.H. Eisen, Radiation Eff.7,129(1971).

36. T.J. Magee, ONR Technical Report, Contract No. 00014-80-0071, July, 1980.

37. T.J. Magee, C. Leung, H. Kawayoshi, B.K.Furman, C.A. Evans, Jr. and D.S. Day, Appl. Phys. Lett. (1981)(in press).

38. M.D. Rechtin, P.P. Pronko, G. Foti, L. Csepregi, E.F. Kennedy and J.W. Mayer, Phil. Mag.(A) 37, 605 (1978).

39. S.U. Campisano, G. Foti and M. Servidori, Appl. Phys. Lett. 36, 279 (1980).

APPENDIX I : TECHNICAL REPORTS PUBLISHED

1. ARACOR Technical Report G-200, "Chromium Depletion Channels and Device Applications," (June, 1980).

2. ARACOR Technical Report G-201, "Field Enhanced Diffusion of Cr in GaAs," (September,1980).

3. ARACOR Technical Report G-202, "Anomalous Diffusion of Oxygen in CZ-Si," (October,1980).

4. ARACOR Technical Report G-203, "Enhanced Diffusion of Cr in InP," (October,1980).

5. ARACOR Technical Report G-204,"Back Surface Gettering Procedures for InP," (Novemeber, 1980).

6. ARACOR Technical Report G-205,"Diffusion and Gettering of Oxygen in Si - Implications for VHSIC Processing," (February, 1981).

7. Interim Report, ONR Contract No. N00014-80-C-0482, Nov.1, 1980.

8. ARACOR Technical Report G-206, "Gettering of CdTe," (March, 1981).

DISTRIBUTION LIST - TECHNICAL REPORTS
Contract No. N00014-80-C-0482

DARPA
1400 Wilson Blvd.
Arlington, VA 22209
(Attn: Program Management). 2

Office of Naval Research 6
Code 427Y
800 North Quincy Street
Arlington, VA 22217

Naval Research Laboratory
4555 Overlook Avenue, S.W.
Washington, D.C. 20375
Attn: Code 2627 6
6800 1

Office of Naval Research 1
Branch Office
1030 East Green Street
Pasadena, CA 91101

TACTEC 1
Battelle Memorial Institute
505 King Avenue
Columbus, OH 43201

Defense Contract Administration
Services 1
Management Area San Francisco
1250 Bayhill Drive
San Bruno, CA 94066

Defense Documentation Center 12
Building 5, Cameron Station
Alexandria, VA 22314

Dr. Y. S. Park
AFAL/DHR
Building 450
Wright-Patterson AFB
Ohio 45433

ERADCOM
DELET-M
Fort Monmouth, NJ 07703

Texas Instruments
M.S. 105/W. Wisseman
P. O. Box 5936
Dallas, TX 75222

Commanding Officer
Office of Naval Research
Branch Office
1030 East Green Street
Pasadena, CA 91101

Dr. M. Malbon/M.S. 1C
Avantek, Inc.
3175 Bowers Avenue
Santa Clara, CA 94304

Mr. R. Bierig
Raytheon Company
28 Seyon Street
Waltham, MA 02154

Dr. R. Bell, K-101
Varian Associates, Inc.
611 Hansen Way
Palo Alto, CA 94304

Dr. H. C. Nathanson
Westinghouse Research and
Development Center
Beulah Road
Pittsburgh, PA 15235

Dr. F. Blum/Dr. Daniel Chen
Rockwell International
Science Center
P. O. Box 1085
Thousand Oaks, CA 91360

Mr. G. J. Gilbert
MSC
100 Schoolhouse Road
Somerset, NJ 08873

Dr. C. Krumn
Hughes Research Laboratory
3011 Malibu Canyon Road
Malibu, CA 90265

Mr. Lothar Wandinger
ECOM/AMSEL/TL/IJ
Fort Monmouth, NJ 07003

Dr. Harry Wieder
Naval Ocean Systems Center
Code 922
271 Catalina Blvd.
San Diego, CA 92152

Dr. William Lindley
MIT
Lincoln Laboratory
F124A, P. O. Box 73
Lexington, MA 02173

Mr. Sven Roosild
AFCRL/LQD
Hanscom AFB, MA 01731

Commander
U.S. Army Electronics Command
V. Gelnovatch
(DRSEL-TL-IC)
Fort Monmouth, NJ 07703

RCA
Microwave Technology Center
Dr. F. Sterzer
Princeton, NJ 08540

Hewlett-Packard Corporation
Dr. Robert Archer
1501 Page Mill Road
Palo Alto, CA 94306

Watkins-Johnson Company
E. J. Crescenzi, Jr./
K. Niclas
3333 Hillview Avenue
Stanford Industrial Park
Palo Alto, CA 94304

Commandant
Marine Corps
Scientific Advisor (Code AX)
Washington, D.C. 20380

Microwave Associates
Northwest Industrial Park
Drs. F. A. Brand/J. Saloom
Burlington, MA 01803

Commander, AFAL
AFAL/DHM
Mr. Richard L. Remski
Wright-Patterson AFB, OH 45433

Professor Walter Ku
Phillips Hall
Cornell University
Ithaca, NY 14853

Commander
Harry Diamond Laboratories
Mr. Horst W. A. Gerlach
2800 Powder Mill Road
Adelphia, MD 20783

Advisory Group on Electron
Devices
201 Varick Street, 9th floor
New York, NY 10014

D. Claxton
MS/1414
TRW Systems
One Space Park
Redondo Beach, CA 90278

Professor L. Eastman
Phillips Hall
Cornell University
Ithaca, NY 14853

AIL TECH
612 N. Mary Avenue
Sunnyvale, CA 94086
Attn: D. G. Vendelin

Professors Hauser and Littlejohn
Department of Electrical Engr.
North Carolina State University
Raleigh, NC 27607

Professor Irving Kaufman
Electrical and Computer Engineering
Arizona State UNiversity
Tempe, Arizona 85281

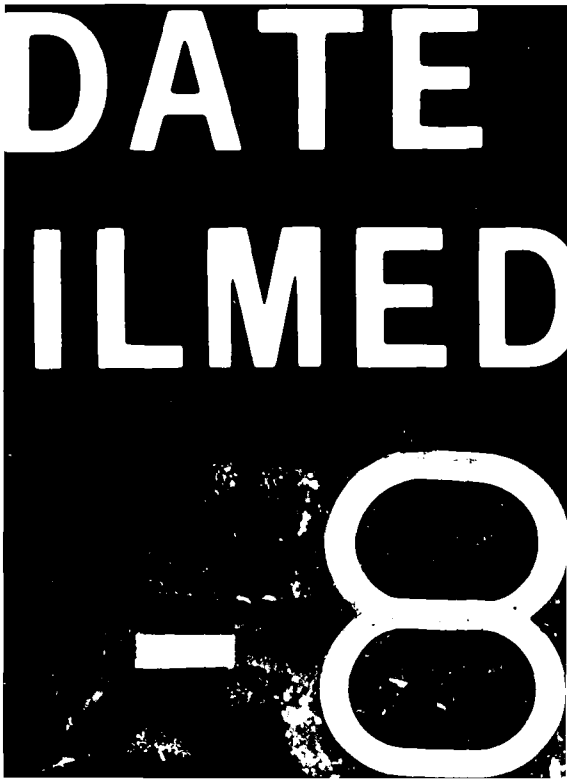
DATE
ILMED
-8